

UW-22 ALBATROSS



HuskyWorks 2021-2022

AIAA Design, Build, Fly

W UNIVERSITY *of* WASHINGTON



Contents

1	Executive Summary	4
2	Management Summary	5
2.1	Team Organization	5
2.2	Milestone Chart	5
3	Conceptual Design	6
3.1	Mission Requirements and Constraints	7
3.2	Sensitivity Analysis	9
3.3	Subsystem Design Requirements	11
3.4	Configuration Selection	12
3.5	Final Conceptual Design Configuration	16
4	Preliminary Design	16
4.1	Design Methodology	16
4.2	Design Trade Studies	17
4.3	Aerodynamics	19
4.4	Aircraft Stability Analysis	23
4.5	Predicted Aircraft Mission Performance	25
5	Detailed Design	27
5.1	Dimensional Parameters	27
5.2	Structure Characteristics and Capabilities	27
5.3	Subsystem Design	27
5.4	Aircraft Flight and Mission Performance	35
5.5	Weight and Balance	36
5.6	Drawing Package	36
6	Manufacturing Plan	41
6.1	Manufacturing Processes Investigated	41
6.2	Manufacturing Processes Selected	42
6.3	Manufacturing Schedule	47
7	Test Plan	48
7.1	Test Schedule	48
7.2	Testing Objectives	48
7.3	System Testing	49
7.4	Flight Tests	51
8	Performance Results	54
8.1	Demonstrated System Performance	54
8.2	Flight Performance	56
9	References	60

Nomenclature

Abbreviations

- ac: Aerodynamic Center
- AIAA: American Institute of Aeronautics and Astronautics
- APC: Advanced Precision Composites
- APD: Advanced Power Drives
- AVL: Athena Vortex Lattice
- BEC: Battery Elimination Circuit
- CAD: Computer Aided Design
- CG: Center of Gravity
- CNC: Computer Numerical Control
- ESC: Electronic Speed Controller
- FEA: Finite Element Analysis
- GA: Genetic Algorithm
- GM: Ground Mission
- IMU: Inertial Measurement Unit
- LiPo: Lithium-Polymer Battery
- M#: Mission Number
- MTOW: Max Takeoff Weight
- NACA: National Advisory Committee for Aeronautics
- NiCd: Nickel Cadmium Battery
- np: Neutral Point
- OpenVSP: Open Source Vehicle Sketch Pad
- PLA: Polylactic Acid
- PC: Polycarbonate
- PET(G): Polyethylene Terephthalate (Glycol)
- PKG: Package
- PWM: Pulse-Width Modulation
- RX: Receiver
- STOL: Short-Takeoff and Landing
- TO: Topology Optimization
- UW: University of Washington
- VLM: Vortex Lattice Method
- XPS: Extruded Polystyrene

Symbols

- AR : Aspect Ratio
- C_i : Coefficient of Generic Quantity
- D : Drag Force
- e : Oswald's Efficiency
- f : Skin Friction
- FF : Form Factor
- FOS : Factor of Safety
- g : Gravitational Acceleration
- i : Incidence Angle
- L : Lift Force
- m : mass
- N : Syringes per Flight Time
- n : Load Factor
- Q : Interference Factor
- S : Area
- s : Distance
- T : Thrust
- v : Velocity
- W : Weight
- z : Vertical Distance
- α : Angle of Attack (AOA)
- δ : Control Surface Deflection
- ζ : Damping Ratio
- μ_r : Rolling Friction Coefficient
- ψ : Yaw Angle
- τ : Period
- ω : Angular Frequency

Non-Symbol Subscripts

- a: Aileron
- e: Elevator
- f: Flap
- l: Roll Moment
- m: Pitching Moment
- n: Yaw Moment
- TO: Takeoff

1 Executive Summary

This report details the design, manufacturing, and testing of an Unmanned Aerial Vehicle to compete in the American Institute for Aeronautics and Astronautics (AIAA) Design Build Fly (DBF) competition. The objective of the competition is to construct an aircraft capable of carrying a payload of syringes and repeatedly deploying vaccine packages on the ground without setting off 25G shock sensors. The competition mandates that the aircraft stays within 8 ft linear dimensions, that the aircraft does not carry more than 100 Watt-hours of energy, and that the aircraft is not of vertical takeoff or lighter than air configuration. Furthermore, the aircraft must follow codes specified in the Federal Aviation Administration (FAA) part 107 standards and must takeoff within 25 ft for all flight missions.

The Huskyworks team optimized the aircraft, titled the *UW-22 Albatross*, to complete three flight missions and one ground mission. During the ground mission, the team must load and unload Mission 2 and Mission 3 payloads as quickly as possible. The first flight mission demonstrates proof of flight and takeoff within 25 ft. The aircraft must complete three laps unloaded within the span of five minutes. For the second flight, the aircraft is required to carry the Mission 2 payload (syringes) and fly as fast as possible. The third flight requires the aircraft to take off and fly one complete lap, at the end of which the aircraft must land, remotely deploy a vaccine package, and takeoff again. The cycle is repeated until all packages have been delivered or a mission duration of 10 minutes is reached.

Score analysis was performed to help determine the aircraft configuration and payload. It was determined that the number of syringes had the most impact on score, as the number of syringes carried in Mission 2 determined the number of boxes that could be carried in Mission 3. The *Albatross* was designed to carry 60 syringes, with a theoretical max limit of 78 syringes, for Mission 2 and deploy 6 packages for Mission 3.

The *UW-22 Albatross* is designed to maximize competition score through reliability and balance across all missions. The aircraft is 72 in long, has a 96 in wingspan, and weighs 12.5 lb unloaded. It is a dual-boom, high wing configuration with wing taper beginning at the motor mounts. The aircraft will fly Mission 2 with a total weight of 15.3 lb at 82 ft/s in 75 seconds. The aircraft will fly with max takeoff weight for Mission 3 at 15.8 lb, deploying 6 vaccine packages over the course of 7 laps lasting approximately 46 seconds each. The aircraft has a hinged nose and empennage for easy loading and unloading during the ground mission which will be completed in 180 seconds.

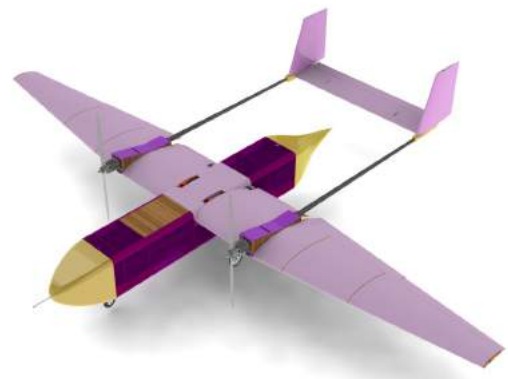


Figure 1: *UW-22 Albatross*

2 Management Summary

HuskyWorks began this 2021-22 competition year with over 130 members, including 36% freshman, 20% sophomores, 29% juniors, 12% seniors, and 3% graduate students. While these students study a variety of disciplines, all team members share a passion for aircraft design. HuskyWorks is led by 10 elected officers who each manage a unique facet of club operations. The team is sponsored by over 22 companies, including MagniX, Eviation Air, Electroimpact, Marymoor R/C Club, and The Boeing Company. These organizations collectively provide substantial monetary and material sponsorship, as well as technical expertise and mentorship through regular Design Review Board meetings.

2.1 Team Organization

The HuskyWorks team has a leadership hierarchy that best facilitates communication and organization. The organization is managed by the Chief Engineer and the Project Manager, and is advised by two faculty advisors who review designs and approve testing activities. The Chief Engineer is responsible for design integration and establishing design constraints. The Project Manager schedules all project timelines and deadlines and manages cross-team communication. The Business Lead is responsible for budgeting, fundraising, marketing, and procurement. Each technical sub-team is run by a sub-team lead, who is responsible for analyzing and defining requirements with the Chief Engineer, ensuring design requirements are met, and adhering to project timelines.

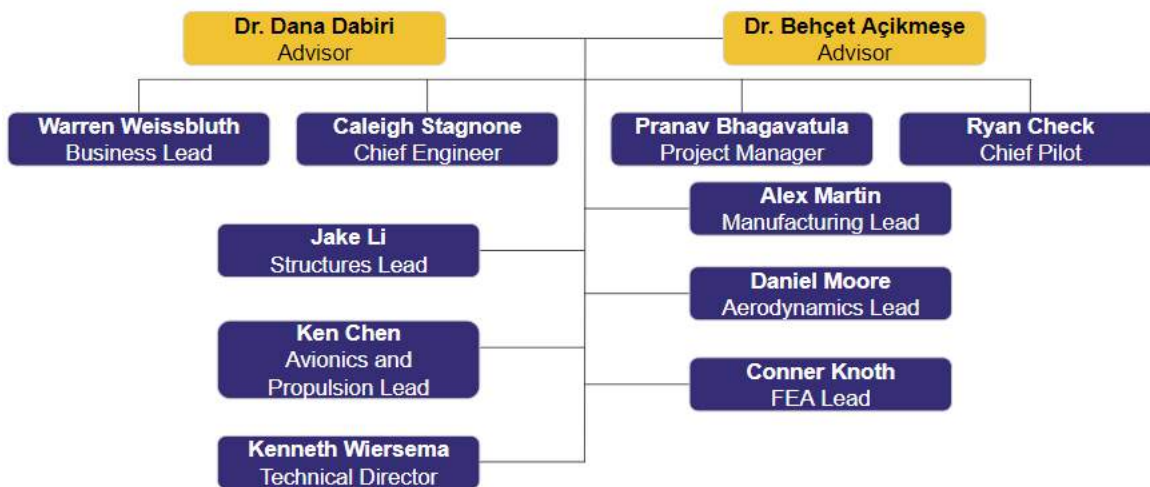


Figure 2: Team Organization

2.2 Milestone Chart

Huskyworks uses a variety of Gantt charts for timeline management. High level charts describe design milestones, administrative deadlines, and provides an overview of the sub-tasks across the project life cycle. Mean-

while, low-level charts focuses on individual sub-task milestones and component deadlines. Fig. 3 is an example of a high-level Gantt chart.

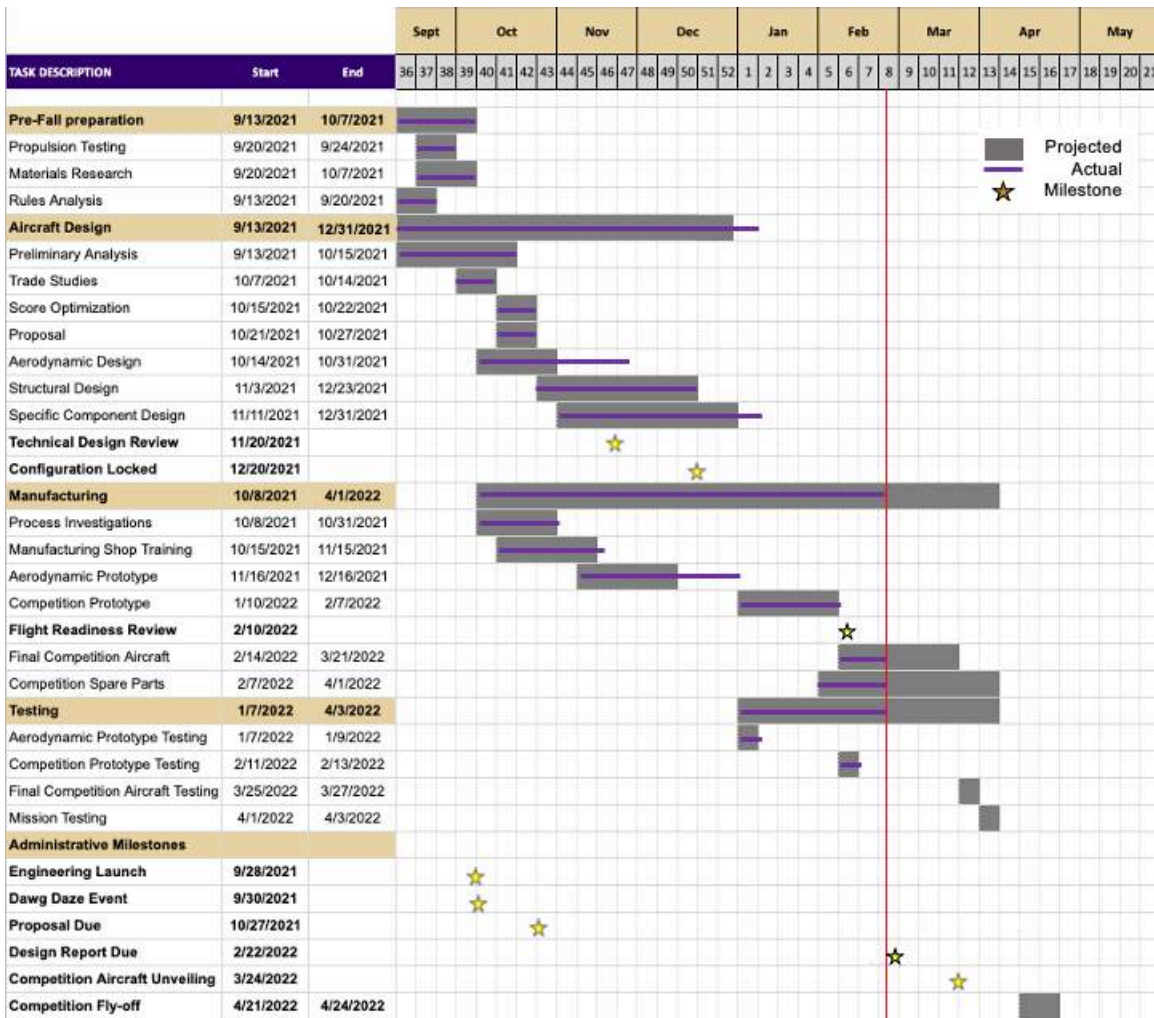


Figure 3: Milestone Gantt Chart

3 Conceptual Design

The 2022 AIAA DBF competition requires teams to design an aircraft to carry 30 mL syringes. Additionally, the aircraft must be capable of storing 2.5 in x 3.0 in x 3.5 in (± 0.13 in) vaccine packages and deploying them such that the attached 25G shock sensors are not set off. This section details the HuskyWorks team’s conceptual design process, resulting in the selection of the aircraft configuration.

3.1 Mission Requirements and Constraints

3.1.1 Competition Scoring Summary

The competition score will be computed using both the Written Report Score and the Total Mission Score as given by Eq. 1.

$$Score = WrittenReportScore \cdot TotalMissionScore \quad (1)$$

Where the Written Report Score is calculated on a 100 point scale based on the quality of the written report. The Total Mission Score is the sum of points from Mission 1 (M_1), Mission 2 (M_2), Mission 3 (M_3), and the Ground Mission (GM) given by Eq. 2.

$$TotalMissionScore = M_1 + M_2 + M_3 + GM \quad (2)$$

Fig. 4 shows the competition lap layout. During each mission, the aircraft must takeoff within a 25 ft runway; time begins for each flight when the throttle is advanced.

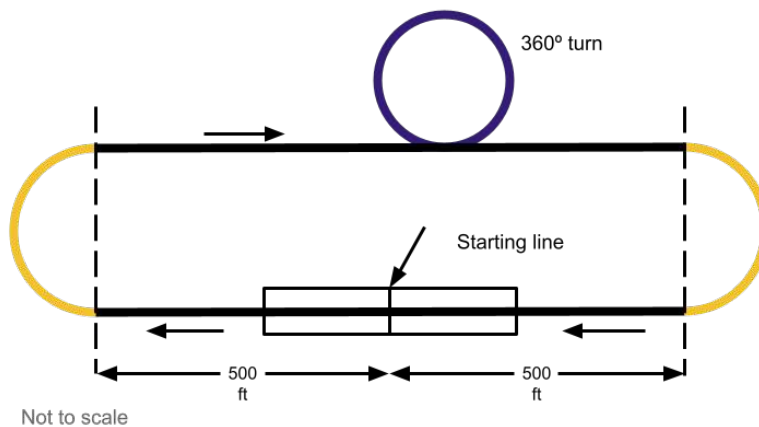


Figure 4: Competition Lap Layout

3.1.2 Mission 1: Staging Flight

Mission 1 teams must complete 3 full laps unloaded within a 5 minute window and with a successful landing. Time ends when the aircraft passes over the finish line in the air. Successful teams will receive a score of 1.0 and unsuccessful teams will receive a score of 0. Eq. 3 shows the M1 scoring.

$$M_1 = 1.0(successful) \quad (3)$$

3.1.3 Mission 2: Payload Flight

Mission 2 requires teams to fly three laps as fast as possible within a five minute window while carrying a payload of syringes. Time ends when the third lap is completed in the air. The minimum number of syringes carried is

10. This mission is scored based on the time it takes to complete the mission and the number of syringes stored. Each team's score is normalized based on the maximum number of syringes divided by the best time scored by a team at competition. The Mission 2 score is given by Eq. 4, where N is the number of syringes divided by flight time.

$$M_2 = 1 + \frac{N_{syringes,UW}}{N_{Syringes,max}} \quad (4)$$

3.1.4 Mission 3: Delivery Flight

Mission 3 requires teams to deliver as many vaccine vial packages as possible within a 10 minute window. The aircraft must fly a standard profile lap until completing the final downwind turn, at which point the aircraft must land on the runway and taxi to the vaccine drop-off site, and remotely deploy one vaccine package. After the package has been deployed, the aircraft must taxi to the start/finish line, come to a complete stop, and takeoff again. This cycle is repeated until all packages have been delivered. Each vaccine package must be retrieved by a Ground Crew Member and returned to the scoring table for evaluation of the shock sensors. If any sensor has been set off, the package will not count. The maximum number of vaccine packages a team may attempt to deliver is the lesser of either the maximum declared during Technical Inspection or the maximum number of syringes flown in a successful Mission 2 divided by 10 rounded down to the nearest whole number. The scoring for this mission is determined by the number of undamaged vaccine packages delivered normalized to the maximum number of packages delivered by a team at competition. Eq. 5 can be used to calculate Mission 3 score.

$$M_3 = 2 + \frac{N_{deployments,UW}}{N_{deployments,max}} \quad (5)$$

3.1.5 Ground Mission: Operational Demonstration

Teams must demonstrate the aircraft's ability to complete Missions 2 and 3 on the ground prior to flight. This mission is timed, beginning when the Ground Mission Official says "GO". At this time, the Assembly Crew Member must load the full Mission 2 payload into the aircraft, after which the Assembly Crew Member must run back to the start/finish line to stop the timer. The timer will be reset, and the assembly crew member must again run to the aircraft when the ground mission official says "GO" and unload the Mission 2 payload. The Crew Member will then replace it with the Mission 3 payload, the timer stopping again when the assembly Crew Member crosses the start/finish line. The Mission 3 payloads must be remotely deployed one at a time and returned to the official to validate system functionality. Failure to deploy the maximum number of vaccine vial packages declared at Technical Inspection will result in an incomplete mission. Scoring for this mission is shown in Eq. 6

$$GM = \frac{t_{min}}{t_{UW}} \quad (6)$$

3.2 Sensitivity Analysis

The sensitivity analysis of the competition aircraft was generated by the Scoring Optimization Algorithm developed by the HuskyWorks team. This provided the team with an multiple outputs; the optimal output was then selected based on viability. The outputs were used as a baseline to generate a parameter sensitivity plot. The following section discusses this two-step process.

3.2.1 Score Analysis

The scoring analysis was approached from a statistical perspective, distinguished from the traditional deterministic point of view, such as solely relying on equation derivations. Specifically, the team developed a mathematical flight model and used a Genetic Algorithm (GA) to optimize it to determine the best configurations under various circumstances. To conclude the analysis, all parameters of each configuration were altered to test their sensitivity to the overall score.

The mathematical flight model was the baseline of the numerical analysis. Following the success of the score optimization project from the previous year, this model was derived with adaptations for 2021-2022 rules. The essence of the model is power balance during the flight, combined with the empirical formulae of peripheral devices obtained from previous years, such as the thrust produced by motors. This model was then outfitted with equations identified in the mission scoring breakdown to create a performance evaluation score. The Ground Mission and Mission 1 parameters were omitted during this analysis because they contribute little to the synoptic scale evaluations. Eq. 7-9 are some representative equations that relate the mathematical model to the competition, with all constants in their SI base unit.

$$L_{course} = \begin{cases} 4 \cdot \pi \cdot \frac{v^2}{a_{max,M2}} + 609.6, M2 \\ 4 \cdot \pi \cdot \frac{v^2}{a_{max,M3}} + 609.6, M3 \end{cases} \quad (7)$$

$$M_2 = \begin{cases} \frac{N_{syringe}}{t_{m2}}, t_{m2} \leq 300 \\ 0, otherwise \end{cases} \quad (8)$$

$$M_3 = N_{lap} = \min \left\{ \frac{600}{L_{course}/v_{M3} + t_{deploy}}, \frac{N_{syringe}}{10} \right\} \quad (9)$$

Unique to the competition in 2021-2022 is the limit of the course length by maximum acceleration during banking. Additionally, the Mission 2 score equation is limited to a time within 300 seconds and the Mission 3 score is constrained either by the syringe payload from Mission 2 or the number of laps. Note that all mission scores are non-dimensional.

After building the mathematical model, the team fed it into the GA to seek out the optimal configurations. GA is a search process inspired by Charles Darwin's theory of natural selection, in which the fittest individual is selected

to reproduce the next generation. Gaussian noise was added to each parameter during the reproduction to mimic the genetic mutation. Next, the mathematical model calculated the entire generation's evaluation score and selected the best. Some random samples (usually not the best ones) from the current generation were selected to pass to the next generation to help the entire generation get out of local maxima. The process was repeated until convergence. GA is also an iterative process, in which the team has to change the hyperparameters and constraints to compare different outputs. Since the mathematical model's convexity is not guaranteed, i.e., multiple local minima existed in the domain, the team started with overestimated constraints, where no individual survived. Then, the harsh restrictions were gradually relaxed until there were acceptable configurations. The team executed each iteration several times to reduce the randomness of the algorithm. The team chose the hyperparameters of simulating 50 generations with a size of 10,000 in which only 500 configurations survived.

Testing the sensitivity of the parameters was also a statistical process. The team introduced a multiplier to all parameters and recorded the score changes for every 500 configurations that survived. The average score changes were plotted in order to serve as general guidance in the latter configuration selection, shown in Fig. 5. Using the values generated by the model, the wing area, lift coefficient, empty weight, and velocity were calculated.

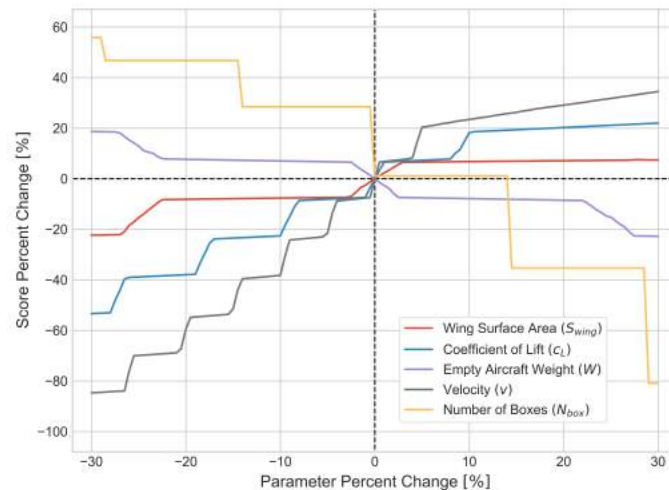


Figure 5: Score Sensitivity of Mission Parameters

3.2.2 Performance Analysis

After accounting for the needed modifications to the GA, the team took the remaining parameters and set them as target values during the preliminary design and configuration selection of the aircraft. The parameters selected drove each design decision during preliminary and detailed design, guiding the design methodology approach.

Table 1: GA Optimized Parameters

Sample No.	Weight (lbs)	v_M2 (ft/s)	V_M3 (ft/s)	c_L	Prop diameter (ft)	power (W)	wing span (ft)	wing chord (ft)	wing area (ft ²)	N_syringe	N_boxes	M2 Score	M3 Score	Total Score
1	20.01	27.21	27.21	0.544	1.257	23.83	8	1.137	8.763	70	7	2	3	5
2	20.01	26.99	26.99	0.448	1.254	34.9	8	1.387	11	69	6	1.982	2.857	4.839
3	20.32	27.03	27.03	0.551	1.4	97.46	8	1.119	8.876	68	6	1.968	2.857	4.826

The GA output a set of suggested performance parameters shown in Table 1. The sensitivity analysis determined that the number of syringes carried in Mission 2 had the greatest impact on competition score, as the number of boxes a team is allowed to deploy in Mission 3 is capped by the number of syringes stored in Mission 2. The maximum score configuration determined by the algorithm is listed in the first row of Table 1, indicating that the optimal aircraft could carry 70 syringes and deploy 7 packages. All configurations were assumed to complete the deployment cycle within 45 seconds.

3.3 Subsystem Design Requirements

The design requirements were developed from the scoring equations and competition guidelines in order to guide the design process. The initial configuration and design approach were guided by an analysis of the scoring equations, selecting configurations to maximize competition score. Competition requirements state the linear dimensions of the aircraft must not exceed 8 ft. Additionally, the aircraft must not be of lighter-than-air configuration or have rotary wings. Propulsion batteries must be NiCad or LiPo, and the propulsion power stored energy cannot exceed 100 Watt-hours. The aircraft must be capable of takeoff within 25 ft and may not switch configurations between missions.

3.3.1 Lifting Surfaces

With a 25 ft takeoff distance, aerodynamic design focused on ensuring the aircraft had enough lift to get off the ground within this distance at all payload and power configurations. It was noted that the critical flights were the first and last flights of Mission 3: the first requires short takeoff with maximum payload and the last requires takeoff with minimum battery power. Optimization studies indicated the need to maximize wing span to increase wing area.

3.3.2 Propulsion System

From the scoring analysis, the endurance target was set at 6 deliveries in M3. After initial calculations, it was determined that the system be designed around the maximum energy limit of 100 Watt-hours, as the increase in propulsion performance significantly outweighs the increase in weight of the system. According to calculations, a 900 Watt average power allowance was determined for M3, besides a 3000 Watt maximum allowance for M2.

3.3.3 Payload

The fuselage was designed surrounding the Missions 2 and 3. Scoring analysis concluded that maximizing the number of syringes stored in Mission 2 greatly impacted the score; thus, the fuselage was designed to maximize the storage capacity. The required length of the Mission 3 mechanism to fit 6 packages and their tolerances determined the length of the fuselage. The mechanism was designed to fit the desired number of boxes at their maximum possible length (3.5 + 0.13 in). The team also paid special attention to the reliability of this mechanism, as it was determined that the ability to successfully complete all deployments during mission 3 depended on the mechanism’s ability to repeatedly make package drops without variance in drop time or mechanism parts failing.

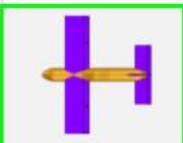
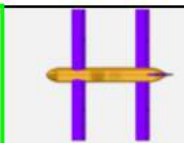
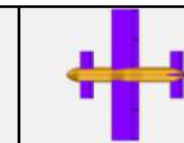
3.4 Configuration Selection

The following section details the design considerations the team completed throughout the conceptual design phase demonstrated via weighted decision matrices. Each figure of merit was assigned a weight between 0 and 1 based on the impact each had on the score. A score between 0 and 10 was assigned to each configuration for each figure of merit, yielding a total score out of 10. The highest score out of 10 was determined to be the optimal configuration. The score for each component was determined through research during trade studies.

3.4.1 Aerodynamic Configuration Selection

For the general aerodynamic configuration of the aircraft, three different configuration ideas were presented: A conventional single wing with horizontal stabilizer, a tandem wing design with two wings, and a tri-surface which had a wing, horizontal stabilizer, and canards located towards the front of the plane. L/D and $C_{D,0}$ for representative models were evaluated in OpenVSP. As summarised in Table 2, the conventional configuration was chosen on the basis of it being a familiar design that was well documented for aerodynamic and control parameters, in addition to having the highest lift. While it had the smallest wing span, that characteristic was judged to be the least important when compared to the complexity of the other two designs. Additionally, the conventional configuration was chosen on the basis that the horizontal stabilizer needed to be located further back on the plane. With the weight restrictions, the conventional design would require the least structural support.




Table 2: Aircraft Configuration Selection Decision Matrix

				
Figures of Merit	Factor	Conventional	Tandem	Tri-Surface
Max Lift / Drag	0.2	10	8	2
Parasitic Drag	0.2	10	7	1
Knowledge Basis	0.3	10	8	3
Wing Span	0.1	3	6	10
Control Complexity	0.2	10	6	3
	Total	9.3	7.2	3.1

3.4.2 Wing Position

For the position of the wing, three different configurations were found, with a low, mid, or high wing, as shown in Table 3. The high wing was deemed to be the most suitable configuration due to it having the highest Lift to Drag ratio and stability, and additionally removing complications with deployment through the bottom of the fuselage that the other two designs would require, and giving the maximum amount of propulsion flexibility by being higher off the ground, allowing for a greater variety of propellers to be used.





Table 3: Wing Position Decision Matrix

				
Figures of Merit	Factor	Low Wing	Mid Wing	High Wing
Max Lift / Drag	0.2	8	9	10
Stability	0.2	5	7	10
Takeoff-Distance	0.2	10	8	7
Payload Interference	0.3	5	6	10
Propulsion Flexibility	0.1	5	7	10
Total		6.6	7.3	9.4

3.4.3 Wing Shape

For the shape of the wing, four different configurations were discussed: straight, tapered, elliptical, and swept. As summarized in Table 4, the tapered wing was chosen due to lower induced drag relative to the straight wing, without adding additional manufacturing complexity. The tapered and swept wings out-scored the elliptical due to manufacturability. The loss of lift with reduced planform for a decrease in drag was acceptable as due to the battery requirements, the aircraft needed to have the lowest possible drag.









Table 4: Wing Shape Decision Matrix

					
Figures of Merit	Factor	Straight	Tapered	Elliptical	Swept
Manufacturing	0.1	10	9	1	9
Lift	0.3	8	6	10	5
Stability	0.2	8	4	8	4
Drag	0.3	2	8	6	8
Complexity	0.1	10	8	1	4
Total		6.6	6.7	6.6	6

3.4.4 Tail Geometry

Stability, versatility, and manufacturability were high priorities when evaluating tail design. Stability of the plane in flight was emphasized, as it was the primary role of the tail. Versatility was the measure of how well the design accommodated the package deployment mechanism. Manufacturability took into account the difficulty of assembling the tail according to the design. Low drag and low weight were prioritized, but less so, due to the tail's relative size to the rest of the plane. Strength was of little concern, due to the low aerodynamic forces relative to the high strength of materials to be used in the tail. Redundancy examined the level of control the plane would have if a control surface was damaged or inoperable, but was not significant enough to warrant a higher factor. Summarized in Table 5, the team initially selected the High Boom configuration due to its high score in versatility and the structural benefits to the dual-boom design. After initial flight testing, the horizontal stabilizer was moved to the base of the vertical stabilizer to improve increase the pitching moment from propwash, so the aircraft could takeoff well within 25 ft.

Table 5: Decision Matrix for Tail Geometry

									
Figures of Merit	Factor	Conventional	Cruciform	High boom	Tri-Surface	T-tail	Twin Boom	V-Tail	Inverted V-Tail
Versatility	0.2	5	7	9	5	9	8	4	2
Stability	0.25	5	4	5	6	4	7	5	7
Low Drag	0.15	5	4	6	6	7	6	7	7
Redundacy	0.05	5	5	5	6	5	5	2	2
Manufacturability	0.2	5	4	5	3	4	5	3	3
Strength	0.05	5	5	8	4	5	8	5	5
Low Weight	0.1	5	4	5	5	3	5	6	6
	Total:	5	4.7	6.25	5	5.45	6.4	4.65	4.7

3.4.5 Propulsion Configuration Selection

The first step was to determine the number of motors to be used (each driving one prop). Following limits set in Section 3.3.3 and other demands, performance metrics were ranked as follows: takeoff thrust, practicality, system lightness, ground clearance, and high speed thrust. Takeoff thrust was of highest priority to ensure the airplane always takes off within 25 ft. Practicality was second, since complications in certain propulsion designs may severely compromise the airframe. Tied for second was system lightness, to aid weight-reduction and overall performance. Ground clearance aids M3 deployment by allowing the airframe to be lower to the ground and help M3 deployment, but was ranked lower due to its lesser impact on improving score. Lastly, any high speed performance that does not compromise completion time of M2 and the number of M3 deliveries was deemed sufficient since a low speed, high energy-efficiency concept was adopted for the airplane. Based on the decision matrix shown in Table 6, the twin-motor configuration was selected. Mounting the motors to each side of the wing in a puller configuration was adopted since it was the most structurally efficient. Additionally, counter-rotating props were adopted, to balance moments and generate outwash, improving stall characteristics.

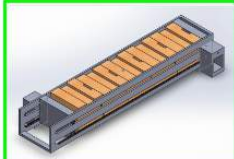
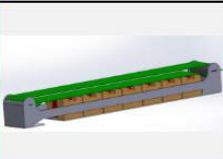

Table 6: Propulsion Decision Matrix with Propellers Listed Below Motors.

Figures of Merit	Factor	Single Motor	Twin-Motor	Tri-Motor	Quad-Motor
		T-Motor AT4130 300KV	T-Motor AT4130 300KV	iFlight X5215 330KV	iFlight X4214 660KV
		APC 20X13 E	APC 20X13 E	APC 16X12 E	APC 12X10 E
Takeoff Thrust	0.35	6	10	8	6
Practicality	0.2	7	10	7	5
System Lightness	0.2	10	8	6	3
Ground Clearance	0.15	3	4	7	10
High-Speed Thrust	0.1	8	6	8	10
Total		6.75	8.3	7.25	6.2

3.4.6 Payload Deployment Mechanism

The weight of the mechanism and speed at which the mechanism could drop packages were the two principle considerations in payload deployment design. The speed at which the deployment mechanism could deploy a package was a principal concern because only ten minutes are allowed to complete all laps and package deployments. Other key factors considered were size, complexity, adaptability to package size tolerances, and ease of manufacturing. Size of the mechanism was considered in terms of both height and length, as these dimensions directly impacted fuselage and aerodynamic design. Complexity was another factor considered, as the more complex the design became, the more points of failure it had, in turn reducing its reliability. Table 7 shows three conceptual designs: the rack and pinion, the conveyor belt, and a mechanism that moved packages in discrete increments. The rack and pinion design scored highly for weight, size, speed, and tolerance adaptability. It was the most compact and appeared to save the most weight. Research and experimentation also suggested it would be capable of dropping packages quickly. By making use of laser cutting and 3D printing, manufacturing this design was relatively simple.

Table 7: Mission 3 Deployment Mechanism Decision Matrix

Figures of Merit	Factor			
		Rack and Pinion	Conveyor Belt	Increment Device
Weight	0.16	7	5	5
Length	0.12	8	6	8
Height	0.14	9	8	5
Complexity	0.14	6	7	5
Speed	0.16	8	8	6
Tolerance Adaptability	0.08	10	9	6
Ease of Programming	0.08	5	9	9
Manufacturability	0.12	7	8	6
Total:		7.5	7.3	6.04

3.5 Final Conceptual Design Configuration

The *UW-22 Albatross* final configuration is dual-boom, high-wing, twin-motor aircraft with tricycle landing gear. The wings were tapered beginning at the motor mounts to provide an optimal lift distribution across the wing and reduce weight at the tips, where the wing experiences the least load. Maximum takeoff performance under any payload is ensured by the twin motors. This aircraft is designed to carry 60 syringes for Mission 2 and deploy 6 vaccine packages for Mission 3. This yields a total payload weight of 2.5 lb and 3.5 lb for Missions 2 and 3, respectively.

4 Preliminary Design

Once conceptual design and trade studies were completed, the HuskyWorks team transitioned into preliminary design, where the aircraft configuration was analyzed and decisions regarding the shape, size, and manufacturing of the aircraft were made. Fig. 6 details a high-level overview of the design process.

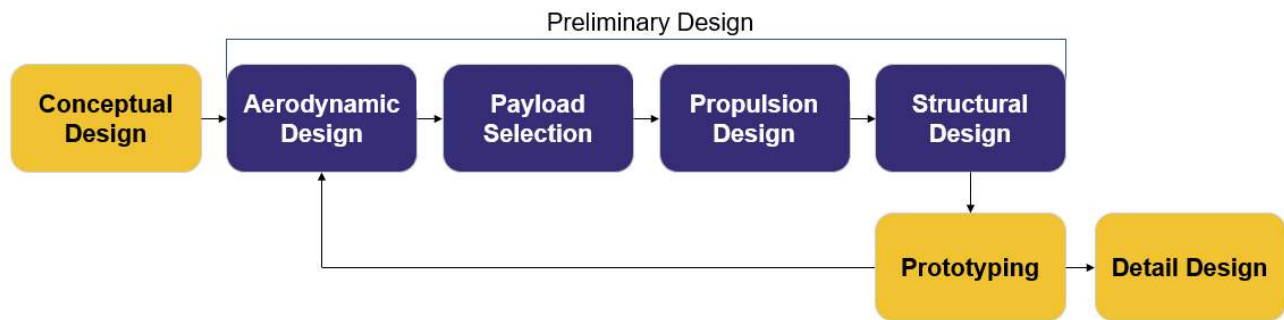


Figure 6: Design Flow Chart

4.1 Design Methodology

At the start of the competition cycle, the HuskyWorks team divided into sub-teams based on team member interest and expertise. The team worked to design an aircraft that maximized payload storage for Mission 2 and flew reliably for Mission 3. The preliminary design began after the desired payload storage capabilities were determined. Through genetic optimization the team determined that it was ideal to deploy 6 vaccine packages for Mission 3 and carry 60 syringes for Mission 2. Based on the payload requirement, the aerodynamics team analyzed several airfoils based on stability, stall angle, lift, and drag that would produce the required lift to takeoff within 25 ft for all flight missions. The structures team focused on weight optimization, identifying a need to move away from a previously used composite monocoque fuselage structure towards a significantly lighter alternative using plywood, balsa wood, and covering film. The propulsion team designed systems to maximize and balance efficiency for both missions. The manufacturing team provided input on the manufacturability of a given design. In order to ensure each design was completed thoroughly, the HuskyWorks team designed the *Albatross* with input from members across all sub-teams.

4.2 Design Trade Studies

Listed in the following section are the trade studies conducted to select the configuration that was optimal for this year's competition. As 6 boxes and 60 syringes were to be stored in the *Albatross*, the trade studies were performed with such a payload in mind.

4.2.1 Tail Sizing

To determine the preliminary size and positioning of the tail, typical tail volume coefficients for general aviation were defined for the initial design; a horizontal tail coefficient of 0.6 and a vertical tail coefficient of 0.06. Using estimates for expected wing reference area, wing mean aerodynamic chord, and location of the center of gravity, definitions of the tail volume coefficients were solved for tail reference area, giving initial estimates for the size of the horizontal and vertical stabilizers. Due to calculations done by the propulsion team based on 20 in diameter propellers, the booms were designed to be spaced 2.25 ft apart on the aircraft. The horizontal stabilizer was then sized to have a span of 2.25 ft, to line up with the tail booms and taking into account the fuselage diameter. A wing-tail ac distance of 36 in was selected, balancing reduction in tail area and maintaining sufficient stabilizer thickness for manufacturing ease

4.2.2 Control Surface Sizing

Initial control surface sizing and design were done for four primary control surfaces: elevators, rudders, ailerons, and flaps. These were based off of initial wing and tail dimensions available at the time and empirical guidelines (1). For the elevator, span was taken to be 95% of the horizontal stabilizer span and chord was taken to be 25% of the stabilizer chord. For the rudder, span was taken to be 90% of the vertical stabilizer span and chord was taken to be 32% of the stabilizer chord. The ailerons were initially placed spanning from 50% of the wingspan to 90% of the wingspan. Finally, the flaps were designed to reach a design goal for lift coefficient of 2.3 (assuming an uncorrected $1.5 C_{L,max}$ without flaps). The percentage sizes of these control surfaces were based off of preliminary design guidelines obtained by the aerodynamics team.

4.2.3 Propulsion Sizing

As described in Section 3.4.3, propulsion optimization was completed for each configuration before the choice of configuration was made. This section focuses on the development of the twin-motor, as it was the final selection; however, the sizing process was the same for all configurations. Continuing from the decision to utilize the full 100 Watt-hour energy limit, the motor and prop combinations were investigated according to the order of weighted performance metric, while staying within the 900 Watt average power allowance for M3 and the 3000 Watt power limit for M2. Additionally, anticipating the demand of counter-rotating props to counter moments on a twin-motor airplane, the propeller choices were limited to those with makes of both orientations. After comparing more than 20 motor and propeller combinations in propulsion calculator tool eCalc, the T-Motor AT4130 300KV brushless outrunner and the APC 20X13E propeller were deemed to be the most appropriate combination (2).

The 20X13E was the optimal choice, as any propeller of a smaller diameter suffered a deficit of at least 3.3 lb of static thrust per motor, defeating any advantage elsewhere. Any propeller of a larger diameter does not contain a counter-rotating option, which could lead to severe controllability issues due to the size and torque they produce. The T-Motor was considered best as it was the lightest of all motors that can produce high performance on the 20X13E without overheating. Additionally, it has a slim-tall form factor, which is aerodynamically advantageous.

Meanwhile, LiPo was chosen as the propulsion battery formula due to its much higher energy density with respect to other formulas allowed under the regulations. Following the motor and propeller combination, the voltage of a 6S battery was required to extract full potential, and hence the 6S 4500 mAh battery was chosen, landing at 99.7 Watt-hours of energy. With a 1.2 factor of safety applied to eCalc's estimate of 143.5 A combined current at max power, 40C was selected as the minimum discharge rate to enable 180 A of current.

4.2.4 Wing Structure

When determining the optimal wing structure, the HuskyWorks team investigated using a skin-supported carbon fiber wing, XPS foam, XPS foam with fiberglass, and plywood with covering film (monokote). Table 8 was used to compare these options based on manufacturability, strength, weight, and rigidity. Weight was the biggest factor given the requirement for a short takeoff. Next was rigidity, which was important due to the need for the wing to survive a 2.5G wing-tip loading test during the Technical Inspection. Manufacturability was ranked next due to the complexity of the wing taper making some options much more challenging. Strength was ranked last due to the material properties indicating that each material could undergo the forces without breaking. After a combination of testing and research, the team selected an XPS foam and fiberglass wing for the competition aircraft. While initially selecting a pure foam wing and implementing this on the Aerodynamic Prototype, the wing was observed to deflect far too much under a wing-tip loading test on the aircraft at its empty weight. Thus, the decision was made to reinforce the wings with 0.75 oz fiberglass. While carbon fiber wings and plywood/covering film wings had benefits in rigidity and weight respectively, the downsides of the carbon fiber's weight and plywood/covering film's manufacturability and rigidity yielded a lower total score.

Table 8: Wing Structure Decision Matrix

Figures of Merit	Factor	Carbon Skin	XPS Foam + Fiberglass	Plywood + Monokote	Pure Foam
Manufacturability	0.25	3	7	5	8
Strength	0.15	9	7	6	2
Weight	0.35	3	5	7	8
Rigidity	0.25	8	6	5	3
	Total	5.2	6.1	5.9	5.9

4.2.5 Fuselage Structure

The HuskyWorks team investigated monocoque and semi-monocoque fuselage structures for the *Albatross*. The two structures were compared based on weight, payload storage capacity (volume), manufacturability, compatibility with deployment mechanism, cost, strength, ability to take an impact, and manufacturing speed (time). The two highest rankings were compatibility with the mission 3 mechanism and weight. Mission 3 was prioritized due to the fact that the fuselage was designed around the mechanism. Weight was important because of the 25 ft takeoff distance limit. Volume had the second largest factor, as the sensitivity analysis indicated that an ability to carry more syringes would have the highest impact on competition score. Time, manufacturability, cost, and impact resistance were notable factors, however, they had little impact on the decision. While the monocoque structure increased payload storage capacity due to the lack of a need for internal structures and had better reusability (measured by impact resistance), it was more difficult to integrate the deployment mechanism and weighed almost twice as much as the semi-monocoque fuselage. While the semi-monocoque structure did have less internal volume and less impact resistance, the benefits of ease of manufacturing, weight, cost, and time led the team to decide on this structure. A decision matrix summarizing these results is shown in Table 9.

Table 9: Fuselage Structure Decision Matrix

Figures of Merit	Factor	Monocoque	Semi-monocoque
Cost	0.05	4	8
Compatibility	0.2	4	9
Weight	0.2	3	7
Time	0.1	5	6
Manufacturability	0.1	5	7
Volume	0.15	8	4
Strength	0.15	8	5
Impact Resistance	0.05	7	3
	Total	5.35	6.4

4.3 Aerodynamics

4.3.1 Airfoil Selection

Fleshing out the three-dimensional wing design, multiple airfoils, listed in Table 10, were considered from the Airfoil Tools database (3). The initial collection of airfoils were selected from those used in previous years and from those with L/D_{\max} extending over a large α range. From the set, the minimization of C_D at cruise conditions and maximizing $C_{L,\max}$ were prioritized. Drag minimization allows higher airspeed, to which performance is most sensitive, and maximizing $C_{L,\max}$ improves STOL performance, critical to all flight missions. Margins for error with in-flight stall and stability and with manufacturing were further considered. Airfoil ratings for each figure of merit were based on the performance scaling relative to the average value of the figure of merit for all the airfoils (average corresponding to a score of 5).

Table 10: Airfoil Selection Decision Matrix

Figures of Merit	Factor	AH 94-145	CH10	FX 63-137	FX 76-MP-140	NACA 4412	NACA 6412	S1223
Max Lift	0.25	3.7	6.5	4.9	4.7	3.2	4.3	7.8
Drag at Cruise	0.4	6.4	0.2	6.6	5.8	7.0	6.4	2.6
Stall Angle	0.15	1.3	2.9	6.8	6.0	6.9	5.2	6.0
Manufacturing	0.1	10.0	7.0	1.0	6.0	10.0	10.0	1.0
Stability	0.1	4.3	4.2	4.2	3.3	4.7	6.6	4.8
Total		5.1	3.3	5.4	5.3	6.1	6.1	4.5

Airfoil performance were taken from tabulated XFOIL data for $Re = 500,000$, on par with the Reynolds Numbers from previous competition seasons. Using the results from Table 10 the NACA 4412 and 6412 airfoils were selected as possible airfoils. Based on review of the L/D versus α curves, shown in Fig. 7, the NACA 6412 was selected in the end due to its higher and broader L/D peak. To minimize drag in M3, for which flight endurance is most important, a wing incidence angle of 3.75° was selected, providing the M3 lift-coefficient of 0.83 at $0^\circ \alpha$. Finite wing corrections are applied to the airfoil lift-curve slope (4). To simplify analysis symmetric airfoils were chosen for the horizontal and vertical stabilizers of sufficient thickness for manufacturing ease (NACA 0012 and 0008, respectively).

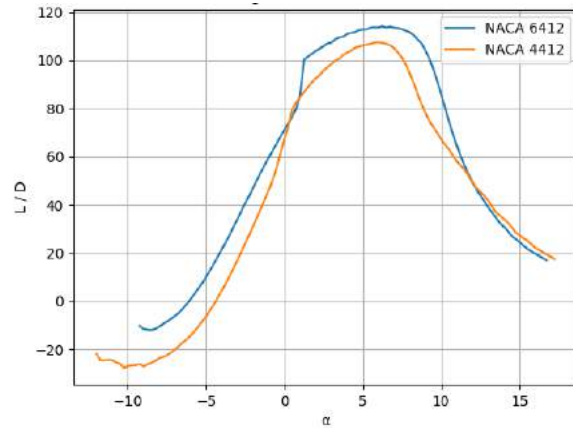


Figure 7: Comparison of NACA 4412 and 6412 L/D

4.3.2 Aircraft Drag Analysis

Lift and drag performance of the *Albatross* were evaluated using the Vortex-Lattice Panel codes available in Mark Drela’s Athena Vortex Lattice (AVL) and the open-source Vehicle Sketch Pad software (OpenVSP) developed by NASA. Both programs are based on linear models and lack viscous boundary-layer subroutines, limiting their accuracy to small angles of attack. OpenVSP’s Parasite Drag Tool was used to estimate the parasitic drag due to each airframe component. Per Eq. 10, this tool evaluates the equivalent skin-friction coefficient (C_f), form-factor (FF), interference factor (Q), and wetted area to calculate the scaled $C_{D,0}$ of each component i (5).

$$C_{D,i} = \frac{S_{wet,i}}{S_{ref}} Q_i C_{f,i} FF_i \tag{10}$$

Using the maximum flight weight and predicted airspeed of the *Albatross* for each mission Eq. 11 was used to estimate the cruise lift coefficient of each mission. These results are included in the predicted performance summary (Table 15).

$$C_L = \frac{L}{qS_{ref}} = \frac{W}{qS_{ref}} \tag{11}$$

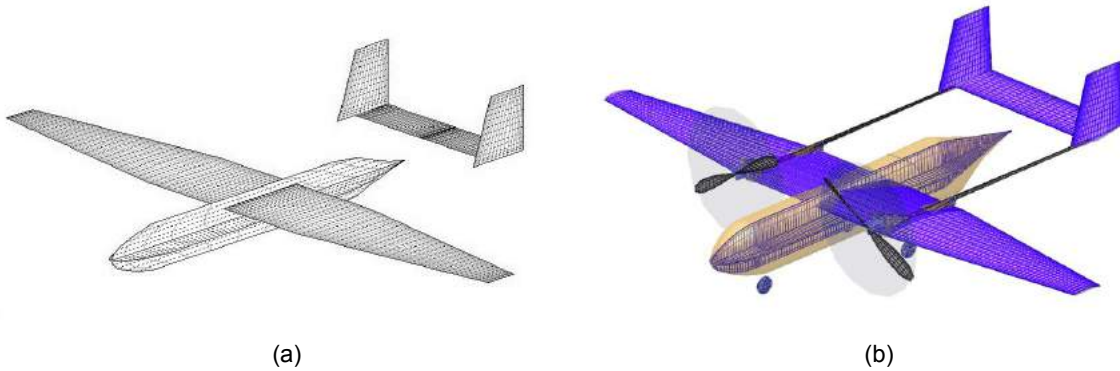


Figure 8: Vortex-Lattice Analysis Models: (a) AVL, (b) OpenVSP / VSPAero

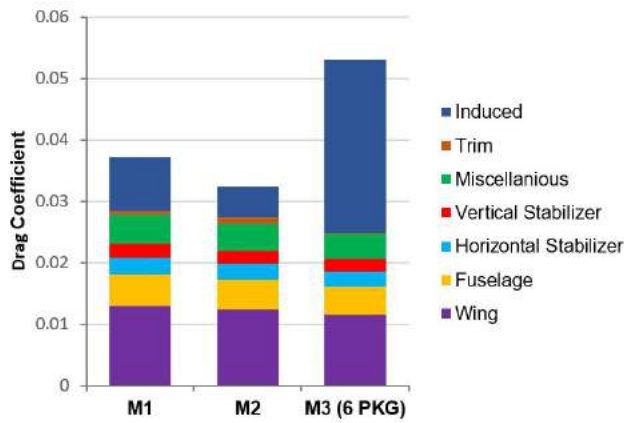
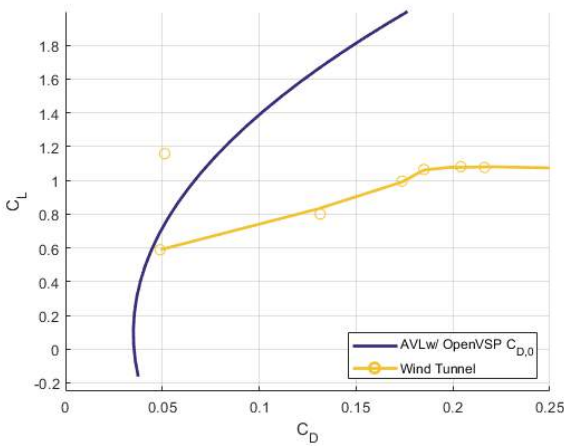
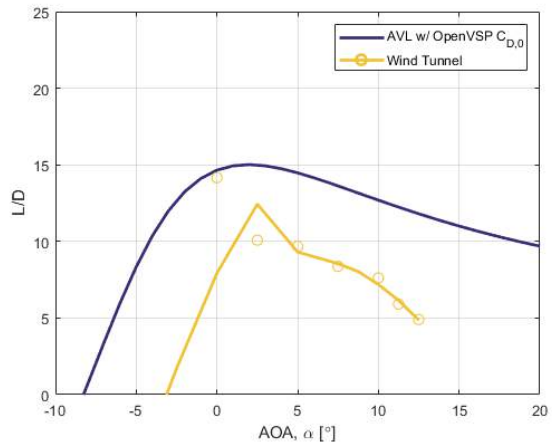


Figure 9: Breakdown of Mission Drag into Components

Control surface deflections and angle-of-attack were trimmed in AVL to yield the required lift coefficient for steady-level flight. This evaluation further calculated the induced drag at cruise. Trim drag was evaluated using the trimmed elevator deflections from AVL and methods from (4), assuming the elevator acts as a dual-direction horizontal-stabilizer flap. The drag-build up for parasitic, induced, and trim drags for each mission are shown in Fig. 9, yielding drag coefficients of 0.037, 0.032, and 0.053 for M1, M2, and M3, respectively.



(a)



(b)

Figure 10: Aircraft Lift and Drag Performance

The drag polar and L/D curve for each VLM model are shown in Fig. 10. The parasitic drag calculated with OpenVSP's Parasite Drag module served as the $C_{D,0}$ for the AVL simulation. Data from the half-body wind tunnel test with 0.18 shift in C_D is shown along the VLM results to highlight the sharp increase drag for viscous, non-linear flows at high C_L . Both experimental and numerical models predict a L/D peak within $2^\circ < \alpha < 3^\circ$.

4.3.3 Wingtip Design

Following primary wing design, the effect of endplates on the wing tips of the *Albatross* was investigated through wind tunnel testing of a 50%-scale half-body. This testing is further detailed in Sect. 7.3.1. The endplates tested, shown in Fig. 12, were designed to fence upper and lower surface flows along the entire chord (a), reduce trailing-edge tip vortex generation (b), and fence upper surface flow and minimize surface area (c). The test setup limited the accuracy of measured drag forces. Fig. 11 indicates little to no improvement in the lift of the *Albatross*. This is likely due to the reduced tip chord size relative to the mean-aerodynamic-chord and thus reduced distance over which air may spill over the tip and contribute to a wing-tip vortex.

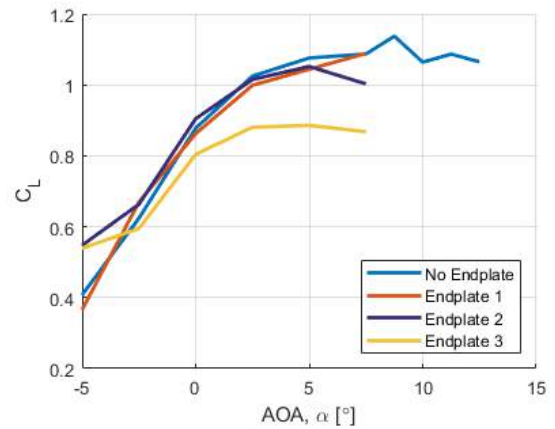


Figure 11: Lift Curve Variation with Endplate

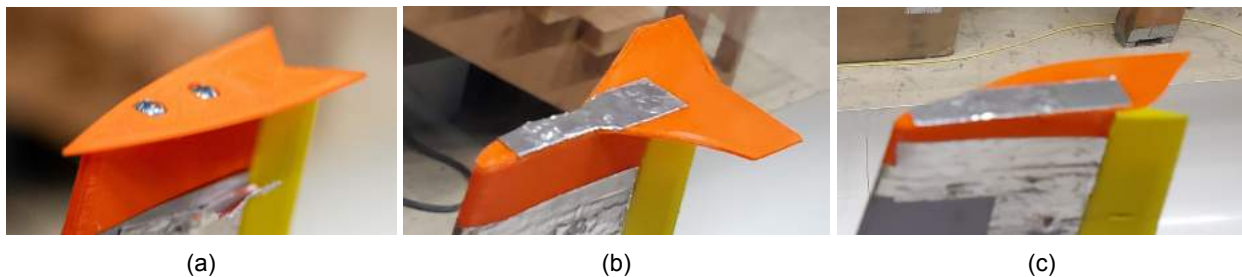


Figure 12: Wing Endplates Tested in Wind Tunnel of Type (a), (b), and (c)

4.3.4 Flap Lift and Drag Analysis

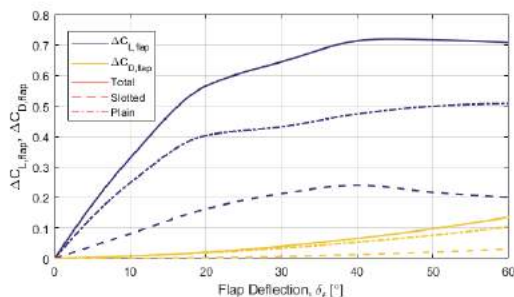


Figure 13: C_L and C_D Change for Individual and Combined Sets of Plain and Slotted Flap Deflection

To help reduce the takeoff distance of the *Albatross*, slotted flaps were selected for the inner flaps between the mounting lines of the motors. Raymer predicts a 44% increase in flap effectiveness for slotted flaps relative to plain flaps (1). Plain flaps were selected for the outer flaps on the tapered section of the wing to reduce manufacturing complexity. Using the empirical methods of (4), Fig. 13 predicts the variation in lift and drag with the deflection of the flaps, as designed.

4.4 Aircraft Stability Analysis

4.4.1 Static Stability

Implementing formulas from (6), a Matlab Script was used to generate figures equivalent to Fig. 14 for multiple horizontal stabilizer incidences. A -4° incidence was chosen, meeting longitudinal static stability requirements and offering a margin for manufacturing error and deviation in the assumed CG position. Accounting for the full aircraft, AVL was used to calculate the principal stability and control derivatives for M2 listed in Table 11, which had the most severe trim conditions. Each stability derivative sign is correct to yield longitudinal, lateral, and directional static stability, with a 0.225 static margin.

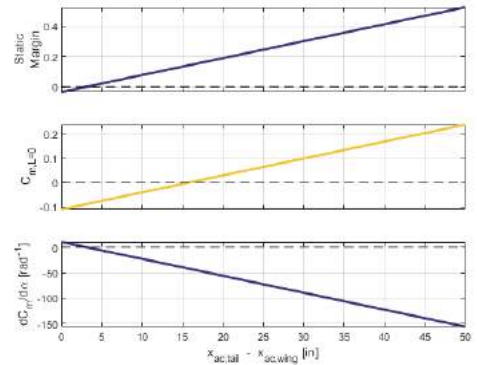


Figure 14: Figures for Horizontal Tail Placement for $b_{tail} = 2.25$ ft, $c_{tail} = 0.455$ ft, and $i_t = -4^\circ$

Table 11: M2 Stability and Control Derivatives Evaluated in AVL

Mission	Stability Derivatives [rad ⁻¹]			Control Derivatives [rad ⁻¹]			
	$dC_l/d\beta$	$dC_m/d\alpha$	$dC_n/d\beta$	$dC_L/d\delta_{r,slot}$	$dC_L/d\delta_{r,plain}$	$dC_l/d\delta_s$	$dC_m/d\delta_e$
M2	-1.160	-69.409	4.272	0.527	1.149	-0.220	-1.389

4.4.2 Dynamic Stability

AVL was utilized to evaluate dynamic mode eigenvalues and damping frequency characteristics. Eigenvalues for both trimmed cruise and trimmed takeoff conditions in Fig. 15 indicate that the Phugoid and Spiral modes are unstable. The other dynamic modes each have negative real parts in their eigenvalues for all conditions. In-line with this indicated stability, the damping coefficient, frequency, and period of oscillations in Tables 12-14 for the Short Period, Dutch Roll, and Roll modes, for all cases, meet the requirements for Level 2 (L2) handling characteristic standards of (7). In this evaluation, the *Albatross* is assumed to mimic a Class II medium weight, low-medium maneuverability aircraft.

For the unstable spiral mode, the mode doubling time falls within Level 3 (L3) requirements for all but M1 takeoff. For the Phugoid mode however, the doubling time is significantly lower than the Level 3 requirement. With the scale of the *Albatross* and increased response rate relative to that of full-scale aircraft, discussion with the pilot determined that the predicted times-to-double are acceptable despite falling outside the guidelines of (7).

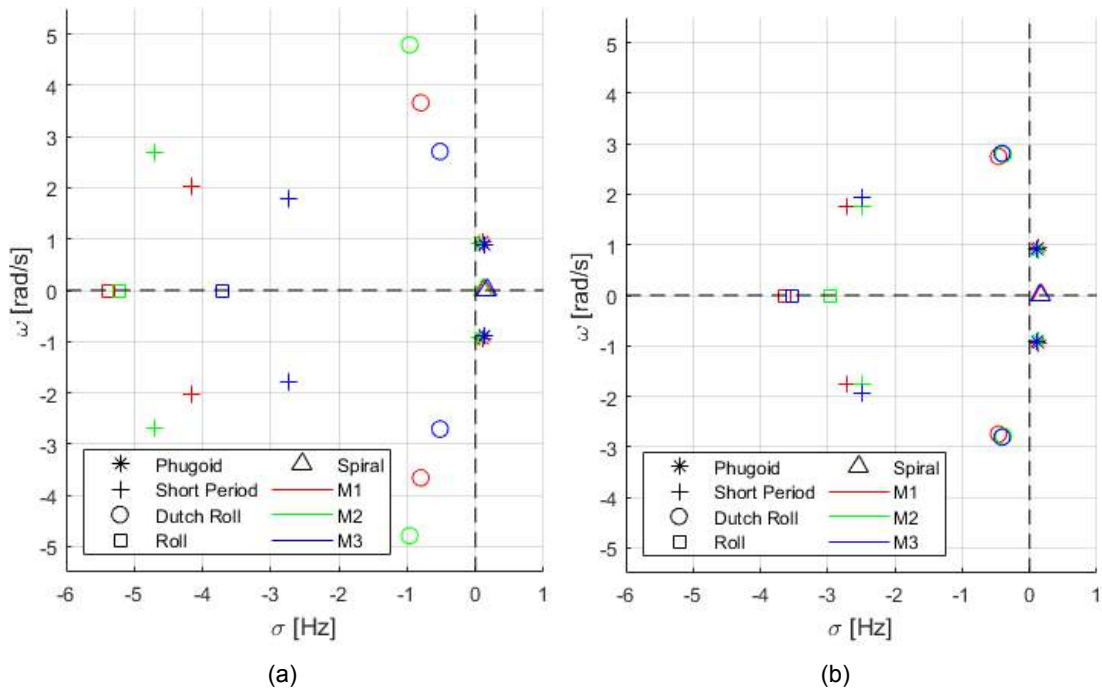


Figure 15: Eigenvalues of Dynamic Stability Modes for Cruise (a) and Takeoff (b)

Table 12: Mission 1 Dynamic Mode Parameters (Cruise/Takeoff)

Dynamic Mode	ζ [-]	ω [rad/s]	$\zeta\omega$ [rad/s]	τ [s]	Double Time [s]
Phugoid	-0.12 / -0.14 < 0 (L2)	0.95 / 0.95	-0.11 / -0.13	6.58 / 6.58	6.20 / 5.28 < 55 (L3)
Short Period	0.90 / 0.84	2.02 / 1.76	1.82 / 1.48	3.11 / 3.57	NA
Dutch Roll	0.21 / 0.17 > 0.02 (L2)	3.66 / 2.75 > 0.4 (L2)	0.78 / 0.45 > 0.05 (L2)	1.72 / 2.29	NA
Roll	1.00 / 1.00	0.00 / 0.00	0.00 / 0.00	0.00 / 0.00 < 3.00 (L2)	NA
Spiral	-1.00 / -1.00	0.00 / 0.00	0.00 / 0.00	- / -	4.99 > 4 (L3) / 3.89 < 4 (L3)

Table 13: Mission 2 Dynamic Mode Parameters (Cruise/Takeoff)

Dynamic Mode	ζ [-]	ω [rad/s]	$\zeta\omega$ [rad/s]	τ [s]	Double Time [s]
Phugoid	-0.06 / -0.14 < 0 (L2)	0.98 / 0.90	-0.06 / -0.13	6.44 / 6.97	9.88 / 5.45 < 55 (L3)
Short Period	0.90 / 0.81	2.74 / 1.77	2.47 / 1.44	2.29 / 3.56	NA
Dutch Roll	0.22 / 0.14 > 0.02 (L2)	6.22 / 2.79 > 0.4 (L2)	1.34 / 0.38 > 0.05 (L2)	1.01 / 2.25	NA
Roll	1.00 / 1.00	0.00 / 0.00	0.00 / 0.00	0.00 / 0.00 < 3.00 (L2)	NA
Spiral	-1.00 / -1.00	0.00 / 0.00	0.00 / 0.00	- / -	6.76 / 4.23 > 4 (L3)

Table 14: Mission 3 Dynamic Mode Parameters at maximum payload (Cruise/Takeoff)

Dynamic Mode	ζ [-]	ω [rad/s]	$\zeta\omega$ [rad/s]	τ [s]	Double Time [s]
Phugoid	-0.16 / -0.12 < 0 (L2)	0.88 / 0.92	-0.14 / -0.11	7.17 / 6.86	4.90 / 6.01 < 55 (L3)
Short Period	0.84 / 0.79	1.79 / 1.95	1.50 / 1.54	3.51 / 3.22	NA
Dutch Roll	0.19 / 0.14 > 0.02 (L2)	2.71 / 2.81 > 0.4 (L2)	0.51 / 0.41 > 0.05 (L2)	2.32 / 2.24	NA
Roll	1.00 / 1.00	0.00 / 0.00	0.00 / 0.00	0.00 / 0.00 < 3.00 (L2)	NA
Spiral	-1.00 / -1.00	0.00 / 0.00	0.00 / 0.00	- / -	4.13 / 4.26 > 4 (L3)

4.5 Predicted Aircraft Mission Performance

4.5.1 Power Curve

Using the parasitic drag estimates from OpenVSP, the idealization of Eq. 12, and thrust versus velocity data from the wind tunnel propeller testing detailed in Section 7.3.2, Fig. 16 was constructed (6). The figure indicates a maximum airspeed of approximately 104.5 ft/s at maximum throttle (corresponding to about 5,000 RPM for the motors).

$$D = qS_{ref}(C_{D,0} + \frac{C_L^2}{\pi eAR}) \tag{12}$$

4.5.2 Takeoff

An analysis of takeoff performance was performed to determine the required flap setting and verify the ability to takeoff within 25 ft for all flight conditions. Assuming the presence of ground effect and a rolling friction coefficient, μ_r of 0.05, the analysis utilized the wind-tunnel predicted thrust and lift curves, used the average parasitic drag across the missions, and required a $1.2v_{stall}$ takeoff speed to ensure a margin for performance error. Variance in lift and drag coefficients with flap deflections were calculated using the methods of (4). From Fig. 17, only for M1 is the aircraft expected to be able to takeoff without flaps, but with an estimated 40° maximum deflection angle, sufficient flap deflection is available for M2 and M3 takeoff.

4.5.3 Turning Performance

Offering insight into the limits of turning performance, the instantaneous turn rate was evaluated for the heaviest loading condition of M3 in Fig. 18. The airframe's corner speed is 71.8 ft/s, corresponding to $85.6 \frac{deg}{s}$. For a given airspeed, Fig. 18 may be used to calculate the instantaneous turn radius according to Eq. 13.

$$r = v/\dot{\psi} \tag{13}$$

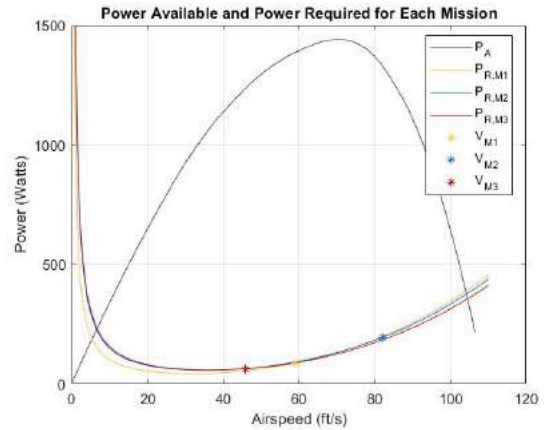


Figure 16: Available and Required Power vs. Airspeed

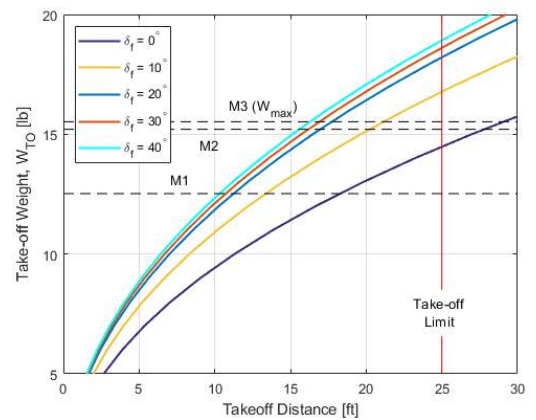


Figure 17: Variation in Takeoff Distance with Weight

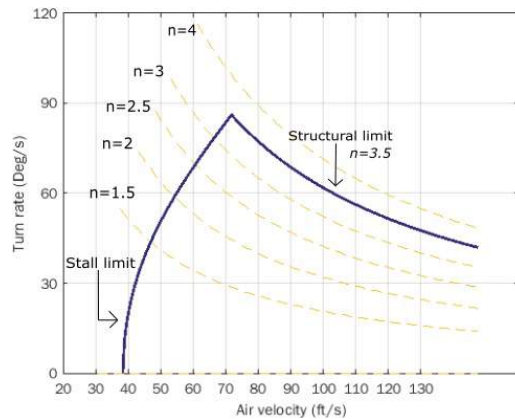


Figure 18: Airframe Turning Rate Performance

4.5.4 Endurance

Fig. 19 shows that With the predicted mission airspeeds of 59, 82, and 46 ft/s, the maximum endurance of the *Albatross* at the maximum mission weights is 13.5, 5.9, and 19.8 minutes, respectively. The predicted mission flight times, tabulated in Table 15 are well within these limits, offering a reserve in battery energy for a non-ideal flight trajectory or the need for a go-around. It may be noted that with the maximum M3 weight with 6 PKGs used, the predicted M3 endurance is a lower bound.

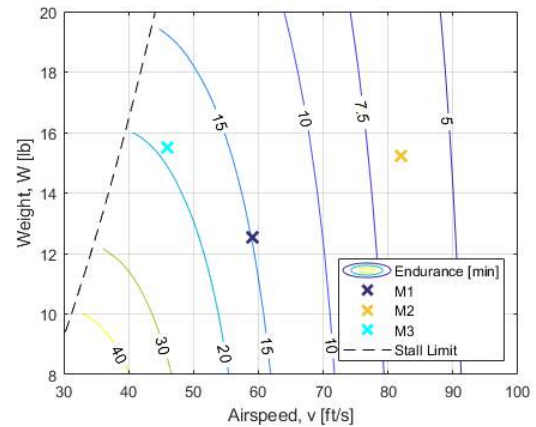


Figure 19: Endurance Variation with Airspeed and Weight

4.5.5 Predicted Performance Summary

Predicted mission-specific flight conditions and performance are summarized in Table 15. The scoring parameters used in the table are the non-normalized flight scores: 1, $\frac{\text{Syringe \#}}{t_{M2}}$, and PKG number for M1, M2, and M3, respectively. It was assumed that landing and taxi-to-deployment, deployment, and takeoff require 15, 20, and 5 seconds, respectively. The M2 and M3 score calculations and weight were based on a predicted 60-syringe and 6 PKG payload, respectively.

Table 15: Predicted Performance of the Albatross

	Mission 1	Mission 2	Mission 3
Weight (lbs)	12.5	15.2	15.5
W/S [lb/ft²]	1.68	2.04	2.08
e [-]	0.72	0.48	0.94
α [°]	-4.57	-6.30	0.37
δ_{elevator} [°]	7.16	8.72	2.68
$C_{L, \text{Cruise}}$ [-]	0.41	0.26	0.83
C_D [-]	0.037	0.032	0.053
L/D [-]	11.1	8.1	15.7
v_{Cruise} [ft/s]	59.1	82.0	45.9
v_{Stall} [ft/s]	37.6	41.4	41.9
$s_{\text{TO}} (\delta_{\text{flap}}=40^\circ)$ [ft]	10.1	15.2	15.9
Turn Radius [ft]	50.3	62.0	64.7
Endurance [min]	13.5	5.9	19.8
Lap Time	44.6	33.9	61.3
Mission Time [min]	2.23	1.69	9.63
Score Parameter	1	1.83	6

5 Detailed Design

The Detailed Design phase takes what was learned and selected during Trade Studies and Preliminary Design to optimize the aircraft. As it has been seen in previous competitions that an aircraft that successfully completes all three competition missions often places within the top 20 teams, the HuskyWorks team focused on aircraft and mechanism reliability during this phase. Sub-system design was iterative to reduce weight and increase efficiency and reliability. Additionally, detailed design carried over into manufacturing as many sub-systems were iterated to optimize performance and improve manufacturability.

5.1 Dimensional Parameters

Table 16 shows the dimensions and electronic components of each aircraft system.

Table 16: Albatross Dimensions and Specifications

Wing		Horizontal Stabilizer		Fuselage		Propulsion		Controls			
Location	Inner	Outer	Airfoil	NACA 0012	Total Length	71 in	Propellers	APC 20 x 13E	Controller	Radiomaster TX16s	
Airfoil	NACA 6412		Span	27 in	Fuselage Length	36 in	Propulsion Battery	SMC Graphene V2 4500mAh 6S 40C	Rx	TBS Tracer Nano RX	
Span	96 in		Chord	6.528 in	Nose length	8 in			Avionics Battery	Lumenier 1300mAh 3S	
Semispan	15 in	33 in	AR	4.13	Empennage Length	13 in	Weight per Pack	1.30 lb	ESC	Mass per Pack	0.216 lb
MAC	1.005		Angle of Incidence	-4 deg	Height	7 in	Model	APD 120F3[X]	Wing Servos	Corona DS 843 MG	
AR	8.585		Vertical Stabilizer	Airfoil	NACA 0008	Width	7 in	Rated Voltage	50.4 V	Deployment Servos	Parallax Feedback 360
Wing Area	55.56 in ²		Number	2	Corner Fillet	0.75 in	Continuous Current	120 A	Propulsion Battery	SMC Graphene V2 4500mAh 6S 40C	
Root Chord	14.4 in	14.4 in	Height	9.72 in	Motor	TMotor AT4130	Mass	0.044 lbs			
Tip Chord	14.4 in	5.05 in	Root Chord	10.068 in	Model	TMotor AT4130	Deployment Mechanism		M3 Controls	Arduino Nano	
Taper Ratio	1	0.35	Tip Chord	6.528 in	Rated KV	300	Deployment Servo	Parallax Feedback 360			
Leading Edge Sweep	0 deg	8.96 deg	MAC	8.304 in	Max Power	1720 W	Ramp Servo	Corona DS 843 MG	M3 RX	Frsky RX8R	
Angle of Incidence	3.75 deg		AR	1.17	Weight	0.893 lbs	Internal Resistance	32 mOhms			
Static Margin (M1, M2, M3)	0.229, 0.225, 0.243		Leading Edge Sweep	20 deg							

5.2 Structure Characteristics and Capabilities

The aircraft has a maximum takeoff weight of 15.57 lb with a load limit of 3.5G. Under such conditions, components were designed to meet structural requirements of 1.5 FOS and mission expectations while minimizing weight. The load experienced by the aircraft is broken down into three parts: aerodynamic loads, propulsive loads, and ground loads. Aerodynamic and propulsive loads act on the wing-tail assembly, transferred through tail booms, wing spars, skin, and mounts to fuselage longerons. Ground loads are dispersed by the main carbon fiber landing gear mounted on fuselage longerons and the nose gear on bulkheads, to create a tricycle configuration.

5.3 Subsystem Design

5.3.1 Package Deployment System

The package deployment system consists of three main components: the frame, the carts, and the ramp. The frame of the package deployment mechanism, pictured in Fig. 20, provides the shape of the mechanism and holds the packages, while the carts, shown in Fig. 21, are responsible for moving the payload onto the ramp for

deployment. The ramp lowers each package onto the runway without triggering the 25G shock sensors.

The side panels of the frame have two slots, an upper slot in which the gears run along the gear racks and a lower slot in which alignment wheels run. Strengthening and alignment came from carbon strips glued to the section of the frame on which the gears run and the fuselage rib structure into which the frame was integrated. Weight savings were achieved by integrating holes into various sections, namely the bottom panel upon which vaccine packages rest. Additionally, spare space in the frame was minimized by allowing the aircraft to house vaccine packages on the ramp during its first lap of Mission 3.

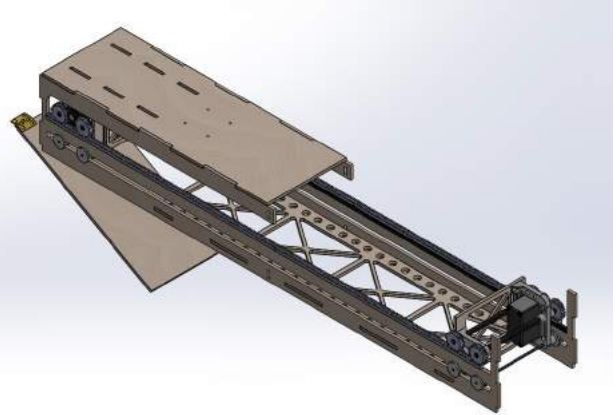


Figure 20: Payload Deployment System

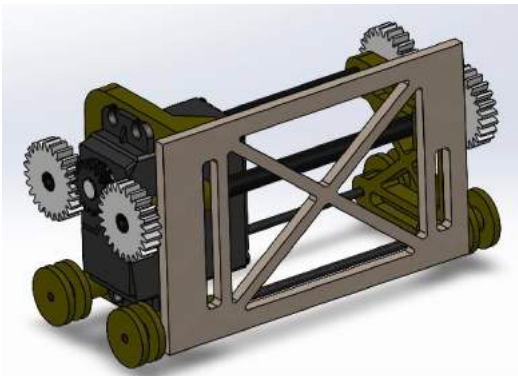


Figure 21: Package Handling Cart

Two carts running along molded nylon gear racks provide the linear actuation required to move the vaccine packages along the payload mechanism. A Parallax Feedback 360° servo was chosen for its high stall torque, high RPM, and positional feedback capabilities. It was determined that when pushing the full weight of six vaccine packages, the Parallax 360° servo would be capable of running at approximately 100 RPM, allowing for the boxes to be moved one box length per second. The gear ratio of the cart actuation was chosen to maintain this desired cart travel speed, while remaining within the servo's torque restrictions. The gears were selected to be 32 pitch as it was necessary for gears to be small enough to fit within the set size of the frame, and large enough to avoid gear slippage due to inaccuracies in construction. Rollers were added to resist the torque generated by the servo, hold the pinion gears against the rack, and keep the carts aligned in the frame.

A bottom mounted ramp was chosen to release packages due to simplicity of operation and effectiveness. The desired angle of the ramp, and by extension, the ramp length, was determined by testing the optimal angle at which the packages would slide down the ramp without triggering the sensors. The ramp was made to open toward the rear of the aircraft for ease of package unloading. The hinge of the ramp was placed well in front of the payload deployment opening to reduce the required opening size to fit a package, as well as reduce the total length of the device. In order to fly with a package on the ramp, the ramp required a robust actuation device that could hold the ramp shut with a package on it during flight. The actuation method was designed such that the

control rod would be parallel to the servo arm in the closed position, minimizing the torque exerted on the servo by the loaded ramp. As an additional precaution, a ramp servo with a sufficiently high stall torque was chosen in order to resist the maximum possible torque when the control rod was perpendicular to the servo arm.

5.3.2 Package Deployment Automation

An Arduino Nano was chosen to control the actuation of the ramp and package handling carts. The Arduino was given a dedicated FrSky RX8R receiver and would be tasked with decoding commands from a radio controller used by the ground crew. The Parallax Feedback 360° servos were powered with 7.2 V from a dedicated BEC. The servo's control wire was connected to a digital pin on the Arduino Nano that supplied a PWM signal. The servo provided the Arduino with a positional feedback PWM signal as well.

Limit switches were placed on each end of the deployment mechanism such that the position of the package handling carts could be zeroed. The cart's exact distance from the switches could then be determined using the servo's positional feedback. This allows the packages to be moved such that the aircraft's center of gravity does not change between package deployments. The ramp servo is also actuated using a PWM signal from the Arduino. The FrSky receiver uses four PWM signals to tell the Arduino when to begin the automatic deployment cycle routine. The Arduino code also includes a manual override that allows the operator to directly control the position of the ramp and carts.

5.3.3 Payload Storage Design

The syringes for mission two are stored vertically on two syringe trays in front of and behind the vaccine package deployment mechanism. These trays are made up of a single panel of foam board with slightly undersized holes such that syringes slide in with a tight fit. The panel can then slide into the front and rear of the aircraft by hinging open the nose cone and empennage. In order to maximize the number of syringes per unit volume, the syringes are stored in alternating fashion such that the flanges of the syringes do not interfere with each other. The vaccine packages are oriented inside the deployment mechanism such that the longest dimension spans the width of the fuselage while the intermediate dimension spans the length of the aircraft. This orientation was chosen to decrease the fuselage length while providing stability to the packages when sliding down the ramp.

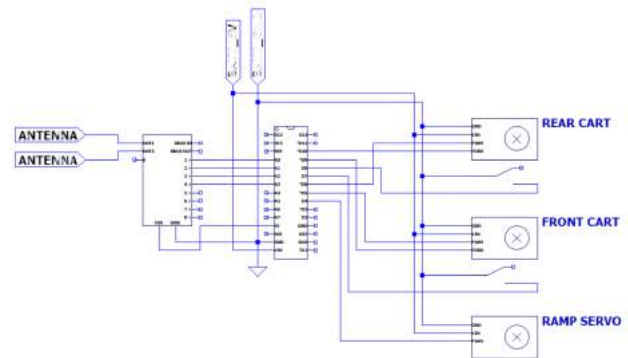


Figure 22: Mission 3 Mechanism Circuit Layout



Figure 23: Syringe Storage Tray

5.3.4 Fuselage Design

The fuselage is a 7 in square cross section with 0.75 in fillets. The structure was composed of 8, 1/8 in plywood ribs and 0.5 in unidirectional carbon fiber spars. Covering film was applied around the ribs for aerodynamics and an access hatch was cut out of the film to access the batteries and flight controller stored above the mission 3 mechanism. 6 of the ribs served as the primary bulkheads, interfacing with other structural members including the M3 mechanism, nose landing gear mount, and syringe storage mechanism. Two additional ribs were included to help maintain the geometry of the fuselage when the covering film was applied. The two spars are located 6 in apart and serve as the primary mounting points for the ribs, rear landing gear and wing.

The first two bulkheads transfer the loads from the nose landing gear mount onto the ribs and longerons, as well as provide support for the deployment ramp. The third and fifth bulkheads are the end plates for the M3 deployment mechanism, and serve primarily to maintain that structure. The fourth bulkhead is located at the aircraft's center of gravity below the first wing spar. The additional two ribs were placed in between the third and fourth, and fourth and fifth bulkheads for geometric shaping. Stringers made of 1/32 in balsa wood curved to the shape of 0.75 in the fillet were included on the fuselage corners to provide sup-

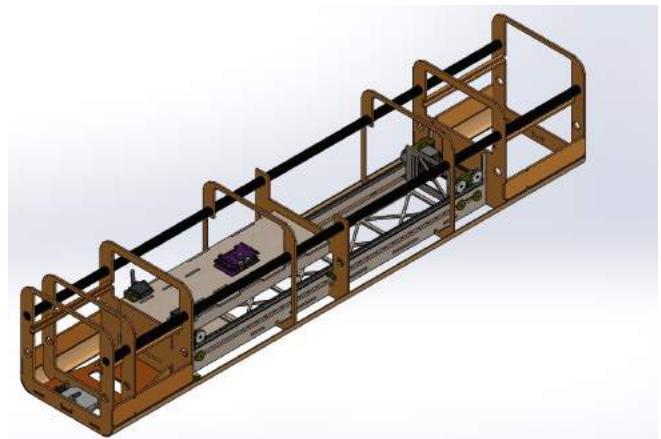


Figure 24: Fuselage Structure with Mission 3 Mechanism

port for the covering film and maintain the shape of the fuselage cross section. The fillets were laid up with 0.75 oz fiberglass to stiffen the stringers. Additional stringers were added between the first and second, and fourth and fifth bulkheads for alignment and additional covering film support.

5.3.5 Wing Design

The wing structure is composed of XPS foam cut into the shape of the airfoil, 0.75 oz fiberglass reinforcement, plywood ribs, and 0.394 in unidirectional carbon fiber spars. As determined in preliminary design, the wing span is 8 ft, divided into three sections separated at the motor mounts. The non-tapered center section spans 27 in with a chord length of 14.4 in. The outer sections of the wing are tapered from a root chord of 14.4 in to a tip chord of 5.05 in. Each side spans 33 in and their structure is identical.

The center wing section is attached to the fuselage via a 3D printed wing mount embedded in the foam that interfaces with four aluminum mounts within the fuselage. The center wing section includes two wing ribs glued onto the wing mount for transferring load from the foam to the spars and wing mount. The side panels of the motor mount offer the load path from the foam to spars on the outer edge of the center wing. Two spars located

at the quarter-chord and $2/3$ of the chord extend out 15 and 5 in from the center section into the outer wings, respectively. 0.75 oz fiberglass was laid up on the surface to provide torsional rigidity and bending stiffness.

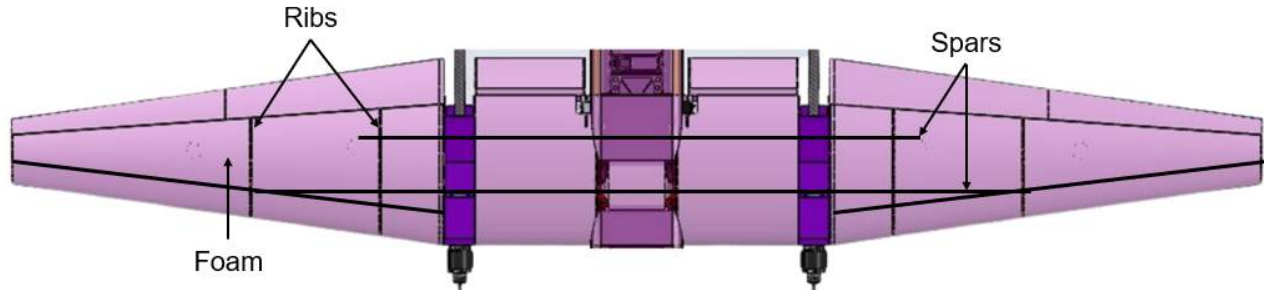


Figure 25: Wing Structure

The outer wing sections consist of one main spar following the taper of the wing along the quarter-chord. 4 ribs were included to distribute the lifting load across the wing. Two ribs were included on either end to provide a load path for the main spar; two ribs were included within the wing section to transfer the bending moment and shear loads to the center section. One layer of 0.75 oz fiberglass was laid up on the wing at a 45° angle to provide torsional rigidity that could avoid tip stall and flutter due to the large wingspan.

The wing has control surfaces along the entire wing span, with slotted flaps adjacent to the fuselage, and separate flaps and ailerons, each spanning 16.5 in as determined in preliminary design. The control surfaces were cut out of XPS foam and 1/32 in balsa wood was laid up on top to provide structural integrity and torsional rigidity. The slotted flaps are attached via a hinges attached to the motor mounts and on one of the wing ribs. The hinges were offset below and in front of the hinge line to provide a gap between the wing and the flaps and to achieve the slotted flap result. FEA simulation was performed on wing structures.

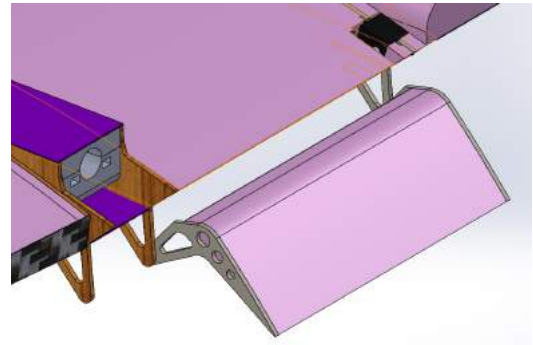


Figure 26: Slotted Flap Mechanism

The simulation indicated that at maximum stress, the structure had a factor of safety of approximately 2 compared to material data. Additionally, a bending test was conducted on the wing tip sections to validate the FEA results due to the complex loading conditions and structural layout.

5.3.6 Wing Mount

The design of the wing mounts was an iterative process. Throughout the design phase, mounts were designed in CAD and reviewed, with an emphasis on weight reduction. Shown in Fig. 27, aluminum mounts were designed in place 3D printed structure, resulting in a 87% reduction in weight while maintaining structural integrity. The wing mount consists of 2 primary components, the 2 upper (PLA) in-wing sections, and 4 CNC machined aluminum

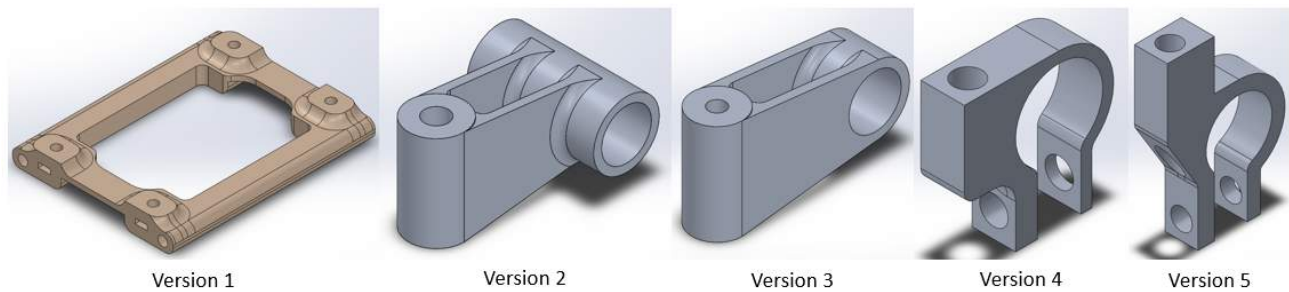
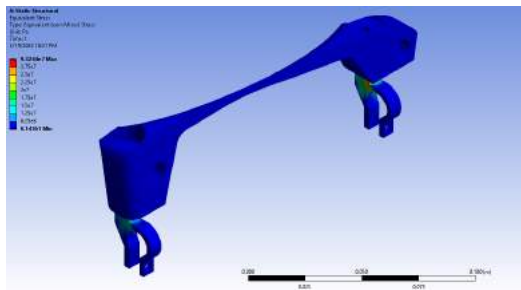


Figure 27: Aluminum Mount Iterations

longeron clamps. The wing spar runs through the embedded wing mount. 4 bolts are fastened from the top through the wing into the 4 longeron clamps. This creates 4 contact points on which the wing loads disperse onto the longerons. During the design process, FEA was used to verify that the wing mount could support the design

loads within a minimum factor of safety and to locate areas of the design that were overbuilt or underbuilt. To simplify the FEA setup, the forces due to the drag and aerodynamic moment on the wing were ignored and the lift force was taken to act perpendicular to the longitudinal axis of the airplane. The lift force applied to the wing mount in the FEA simulations was determined by multiplying the expected 15.57 lb MTOW by the maximum expected load factor of 3.5G and by a 1.5 factor of safety, which yielded a

maximum expected lift load of 58.39 lb. This lift force was distributed equally across the four spar holes in the wing mount.



5.3.7 Motor Mounts

The motor mount structure is designed to act as the transition point between the central wing and the wing tips. Consisting of 2, 1/8 in plywood side panels and a double layered face plate, the assembly includes 2 sets of 3D-printed PLA clamps to secure the motor mount onto wing spars and secure the tail booms. This allowed for both the tail and wing tips to be removed during transport. The 3D-printed tail boom clamp mounted onto the first wing spar also holds servos for the rudders. The side panels act as additional ribs for the wings. Informed by FEA, the motor mount design was iterated to remove unnecessary material and decrease drag. Shown in figure 28, the analysis determined that the plywood back plate was not needed and prone to failure. Additional material was removed on the front plate to save weight and allow for cooling and ventilation of the motors. Covering film was fixed across the top and bottom to reduce drag.

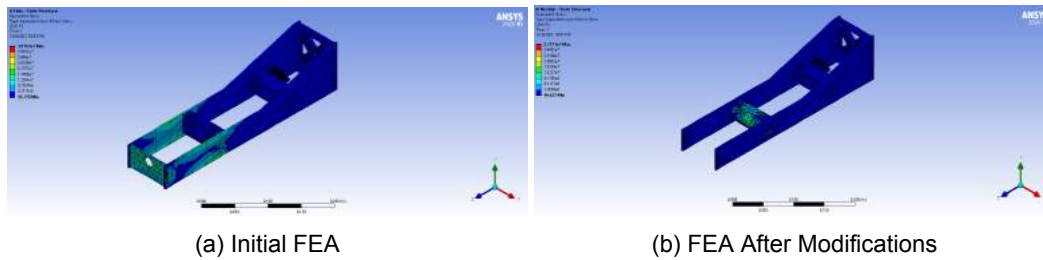


Figure 28: Comparative FEA of Motor Mounts

5.3.8 Landing Gear

The mount was designed to hold the nose gear in place under high impacts while allowing for the wheel to be turned by a servo to steer the aircraft. Given that there are no longerons in the lower half of the fuselage, the mount was designed to fasten between two ribs. Topology optimization was performed as the basis for the design of this component due to the difficult loading conditions. The bounding box was defined as the entire space between the front two ribs that would not interfere with the payload. A stress constraint was placed on the model to ensure that it would not fail and a symmetry constraint was added to make the product easier to manufacture. The objective of the optimization was to minimize the volume and the displacement under maximum load with respective weights of 25% and 75%. The output mesh was smoothed and the part was 3D-printed for testing. The testing led to the addition of holes through which to fasten the mount using screws and a cut-out for placing the steering servo. The topology optimization process is summarized in Fig. 29a.

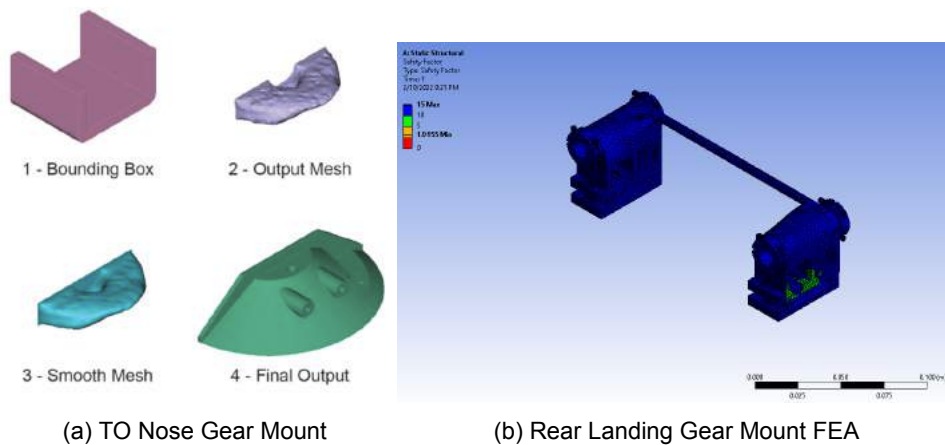


Figure 29: Landing Gear Mounts

The rear landing gear mount also saw many iterations. Initially, the rear landing gear was coupled with the rear pieces of the wing mount. However, upon flight testing, the landing gear was required to move forward in order to increase the pitching moment to takeoff within 25 ft. In order to keep the wing in the same position relative to the center of gravity, the landing gear was de-coupled from the wing mount. Fig. 29b shows the validation of

the new mount, which was weight-optimized after the results of the simulation indicated the inclusion of excess material.

5.3.9 Tail

The tail design took the shape of a twin boom U-tail as determined in preliminary design. The tail booms were two 36 in long unidirectional carbon spars that taper from a diameter of 0.83 to 0.485 in to optimize strength and weight distribution. Constructed similar to the wings, the vertical and horizontal stabilizers are cut to the shape of the airfoil out of XPS foam. One 0.394 in woven carbon fiber spar was used as the primary structural member in the each stabilizer. A short 0.315 in carbon spar was used as an

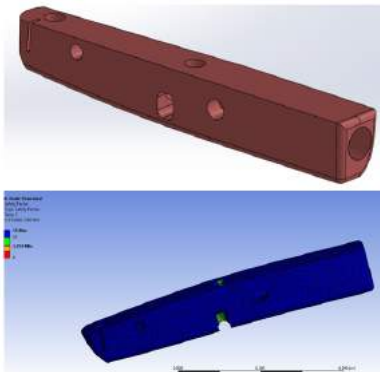


Figure 30: Stabilizer Connectors

additional connecting point between the foam and connector. Connecting the elements of the tail was a 3D printed PLA part that joined tail stabilizers and booms. Objectives of this part are providing rigid connection between tail components and a servo wire routing path. Tail booms were inserted into the connector with servo wires passing through a boom. The connector had two mounting holes on both the vertical and horizontal stabilizer interface for spars. FEA was performed on the tail boom spars to verify the rigidity under maximum aerodynamic load from the tail. The result suggested that under maximum loading from stabilizers, which was 18 lb on two tail boom, one single tail boom would deflect about 0.5° . FEA was conducted on the

connector piece to ensure it's ability to withstand and transfer the load. Applying loads equal to the maximum expected aerodynamic forces from the stabilizers, it was found that the connector would maintain a minimum factor of safety of 3.7, and over 15 for reinforced wire channels, providing sufficient strength.

5.3.10 Nose and Empennage

The nose and empennage for the aircraft were similar in design as their primary purpose was for aerodynamics, as they experience small structural loads. The nose is an 8 in parabolic shape with a filleted square base to interface with the fuselage cross section. Similarly, the empennage was fitted to the square cross section of the fuselage at its base, with a 13.02 in length. Both the nose and the empennage, shown in Fig. 31, were attached using 2 sets of plastic hinges on the top and a locking mechanism on the bottom that was secured using a cotter pin. The nose also included the pitot tube and a plywood mount for 20 syringes, including an array of netting hooks to secure the syringes. The material for the nose was selected to be PET plastic which would be vacuum formed in order to create a durable, lightweight structure; however, the complex shape of the empennage made it necessary to be 3D printed out of PLA. For the nose and empennage shells, FEA was done on the load bearing locking mechanisms. The weakest points analyzed were the 3D-printed cotter pin holes that attached to the fuselage ribs. Using FEA, these locking components were tested over three times the expected weight of the nose and showed to be durable by two orders of magnitude when analyzing stress.

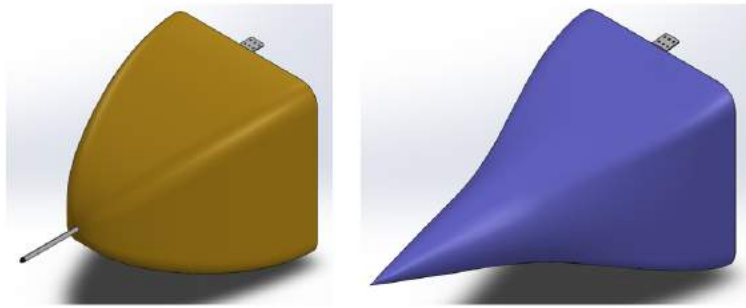


Figure 31: Nose and Empennage Shells

5.3.11 Propulsion

The SMC Graphene Extreme V2 40C battery pack was selected since it was the lightest option and SMC has the best record of accurate C rating as well as high discharge percentage according to “Real C” battery load tests performed by MCSGUY on RC Groups (8). In addition, a 160 A fuse was selected to protect the motors according to data posted by T-Motor (9), since the motors would fail before the battery reaches its maximum discharge of 180 A. Considering the mechanical and electrical punishment during repeated STOL operations, the APD 12S 120 A F3[X] ESC was selected for its extreme robustness. Designed for high continuous power draw of drone racing and surviving high speed crashes, maximum performance and reliability are guaranteed by this ESC, while being more than 0.2 lb lighter than traditional fixed-wing ESCs.

5.4 Aircraft Flight and Mission Performance

Table 17 shows the predicted aircraft performance for each mission using data gathered from previous sections.

Table 17: Predicted Aircraft Performance for each Mission

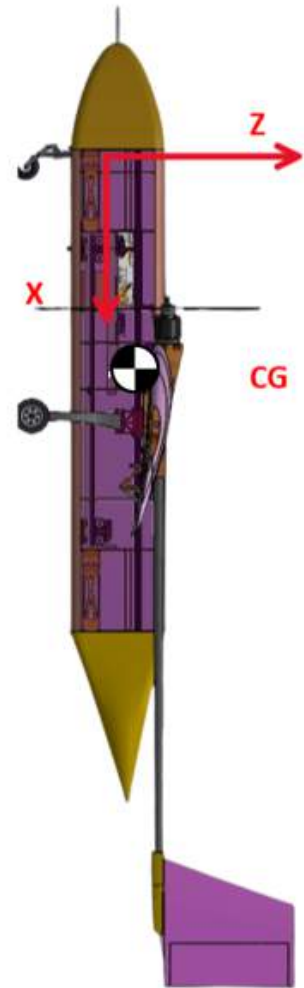
	Mission 1	Mission 2	Mission 3
Weight (lbs)	12.5	15.2	15.5
W/S [lb/ft ²]	1.68	2.04	2.08
e [-]	0.72	0.48	0.94
α [°]	-4.57	-6.30	0.37
δ_{elevator} [°]	7.16	8.72	2.68
$C_{L, \text{Cruise}}$ [-]	0.41	0.26	0.83
C_D [-]	0.037	0.032	0.053
L/D [-]	11.1	8.1	15.7
v_{cruise} [ft/s]	59.1	82.0	45.9
v_{stall} [ft/s]	37.6	41.4	41.9
$s_{\text{TO}} (\delta_{\text{flap}}=40^\circ)$ [ft]	10.1	15.2	15.9
Turn Radius [ft]	50.3	62.0	64.7
Endurance [min]	13.5	5.9	19.8
Lap Time	44.6	33.9	61.3
Mission Time [min]	2.23	1.69	9.63
Score Parameter	1	1.83	6

5.5 Weight and Balance

The *Albatross's* empty weight is 12.52 lb. The center of gravity is located at the quarter-chord of the wing, which sits approximately 26 in back from the tip of the nose cone.

Table 18: CG Table with Frame of Reference

Component	Weight(lb)	X Displacement(in)	Z Displacement(in)
Wing Tips	1.19	20.87	2.39
Tail Assembly	0.74	57.50	5.65
Center Wing	1.34	19.13	2.77
Tail Boom	0.29	34.73	2.89
Fuselage	2.36	14.78	-1.21
Flight Controls	0.18	15.97	0.51
Empennage	0.22	32.24	0.16
Landing Gear	0.60	15.46	-2.76
Motor	1.14	12.94	2.77
Avionics	0.97	14.78	0.00
Battery	1.53	10.51	0.91
Nose	0.22	-2.76	0.00
Motor	1.78	12.94	3.62
CG			
Nose syringes	0.8	3.32	0.00
Front fuselage syringes	1.0	-2.57	0.00
Rear fuselage syringes	1.0	32.81	0.00
6 packages	3	17.87	-2.20
	Weight	X CG	Z CG
M1	12.6	17.91	1.45
M2	15.5	16.74	1.09
M3	15.56	17.90	0.29



5.6 Drawing Package

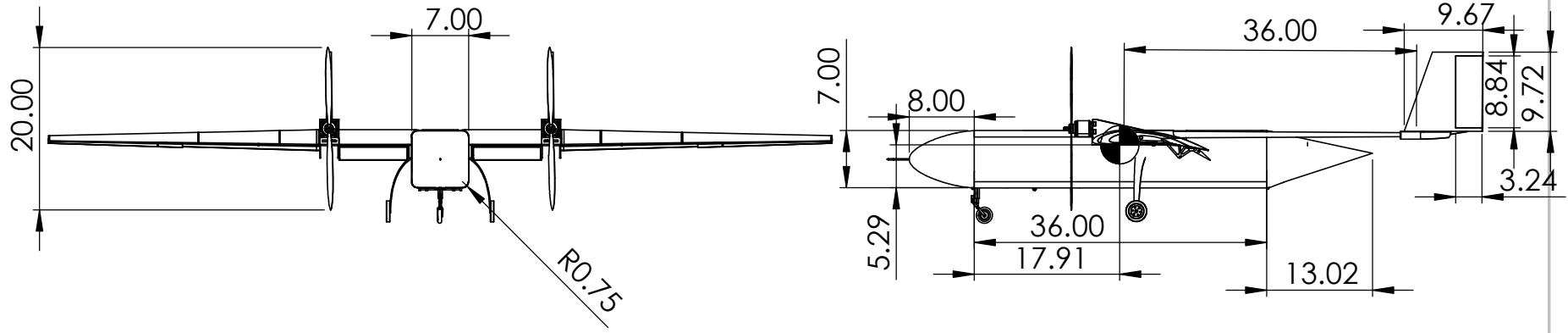
The drawing package contains a dimensioned 3-view of the aircraft, additional views of the primary structure of the aircraft, locations of the electronics within the aircraft, and detailed views of the subsystems of the aircraft.

2

1

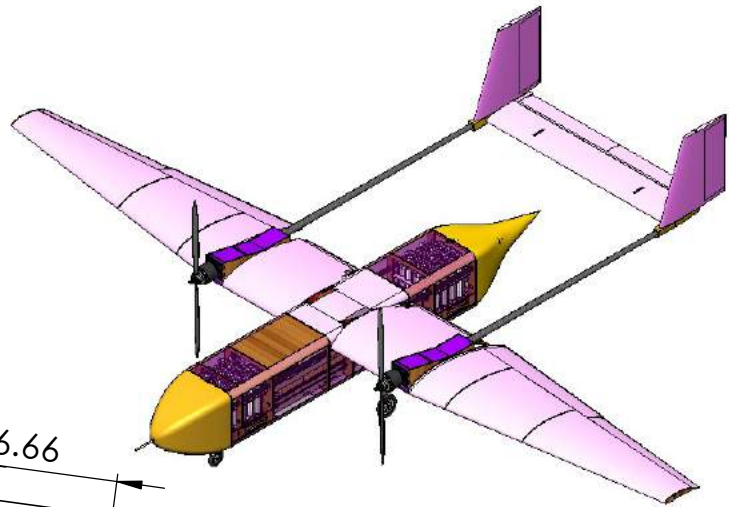
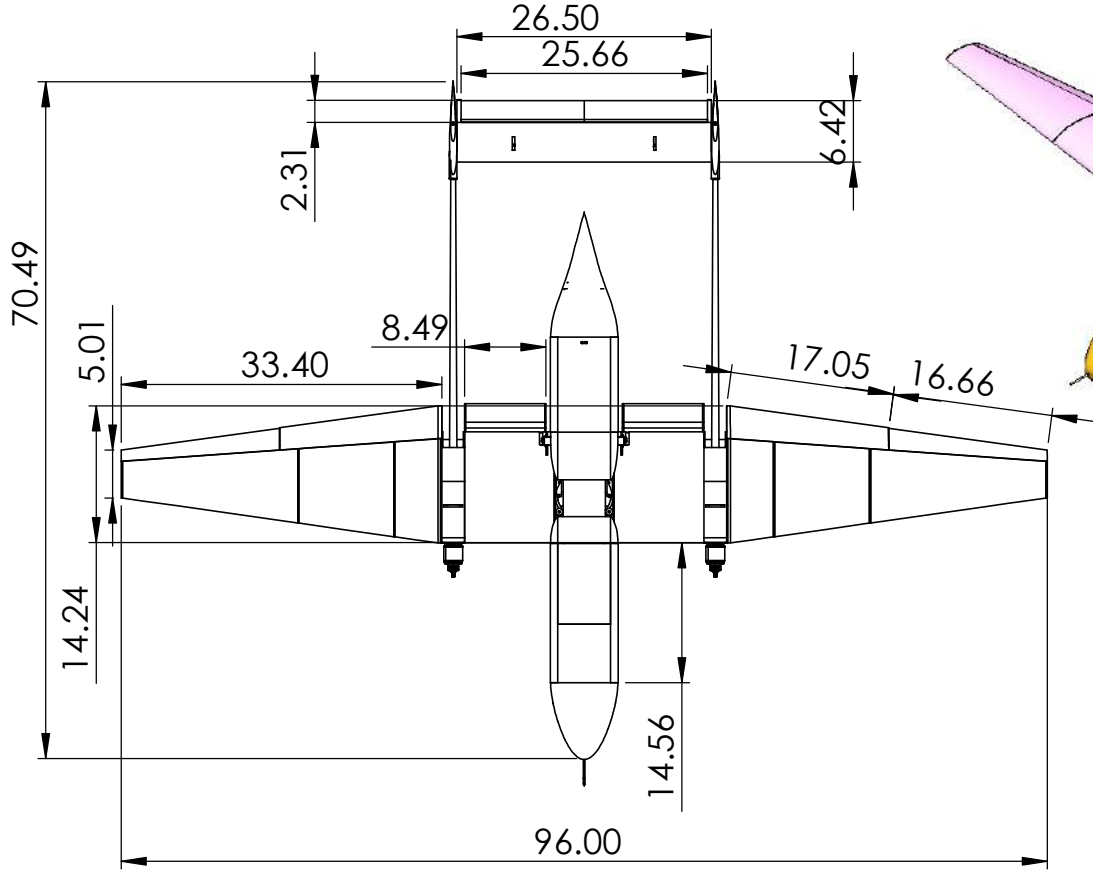
B

B



A

A



UNLESS OTHERWISE NOTED: DIMENSIONS ARE IN INCHES		HuskyWorks
University of Washington Design/Build/Fly 2022		
TITLE: Albatross		
SIZE	DWG. NO.	
A	Aircraft 3-View	
SCALE: 1:20	Drawing Package	SHEET 1 OF 4

1

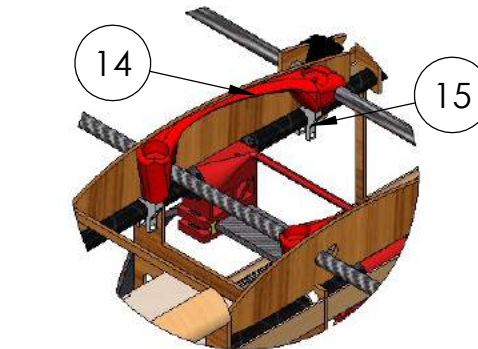
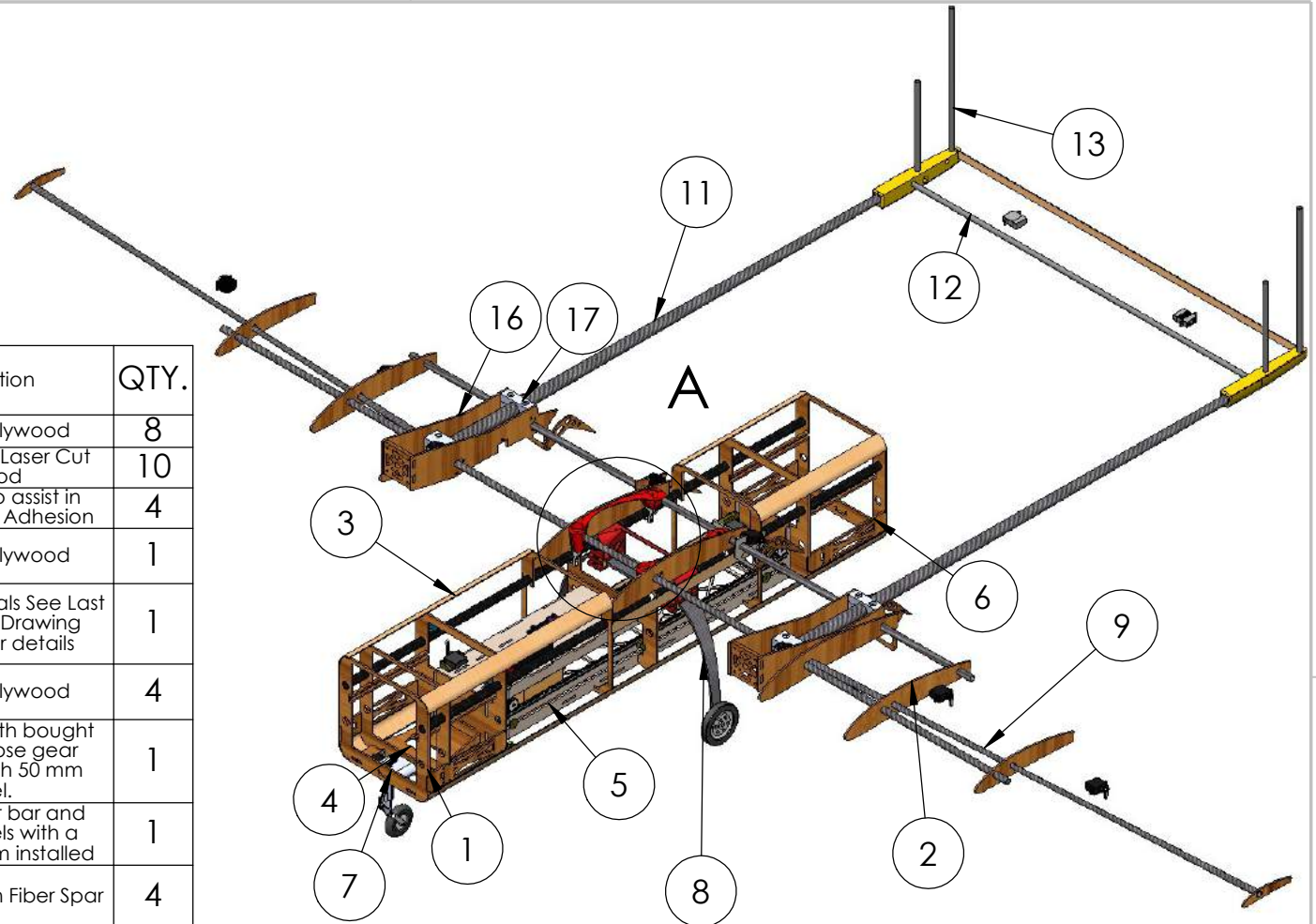
2

1

B

B

Part NO.	Name	Description	QTY.
1	Fuselage Rib	Laser Cut Plywood	8
2	Wing Rib	Varies in size, Laser Cut Plywood	10
3	Skin Support	Bent Balsa to assist in Covering Film Adhesion	4
4	Ramp Mount Panel	Laser Cut Plywood	1
5	Mission 3 Mechanism	Various Materials See Last Page of the Drawing Package for details	1
6	Torsional Stringers	Laser Cut Plywood	4
7	Nose Landing Gear Assembly	PLA mount with bought steerable nose gear assembly with 50 mm wheel.	1
8	Rear Landing Gear	Carbon Fiber bar and 65mm wheels with a braking system installed	1
9	Carbon Fiber Wing Spar	10 mm Carbon Fiber Spar	4
10	Carbon Fiber Fuselage Spar	0.5 in Carbon Fiber Spar 36 in long	2
11	Carbon Fiber Tapered Boom	Varies from 0.83in to 0.485in, 36 in long	2
12	Horizontal Stabilizer Spar	10 mm Carbon Fiber Spar	1
13	Vertical Stabilizer Spar	10 mm Carbon Fiber Spar	4
14	Wing Mount Wing Interface	PLA	2
15	Wing Mount Fuselage Interface	Aluminium	4
16	Motor Mount	Laser Cut Plywood	2
17	Boom Mount	PLA	2



DETAIL A Wing Mount
SCALE 1 : 5

UNLESS OTHERWISE NOTED:
DIMENSIONS ARE IN INCHES

HuskyWorks

University of Washington
Design/Build/Fly 2022

TITLE:

Albatross

SIZE DWG. NO.

A Structural Diagram

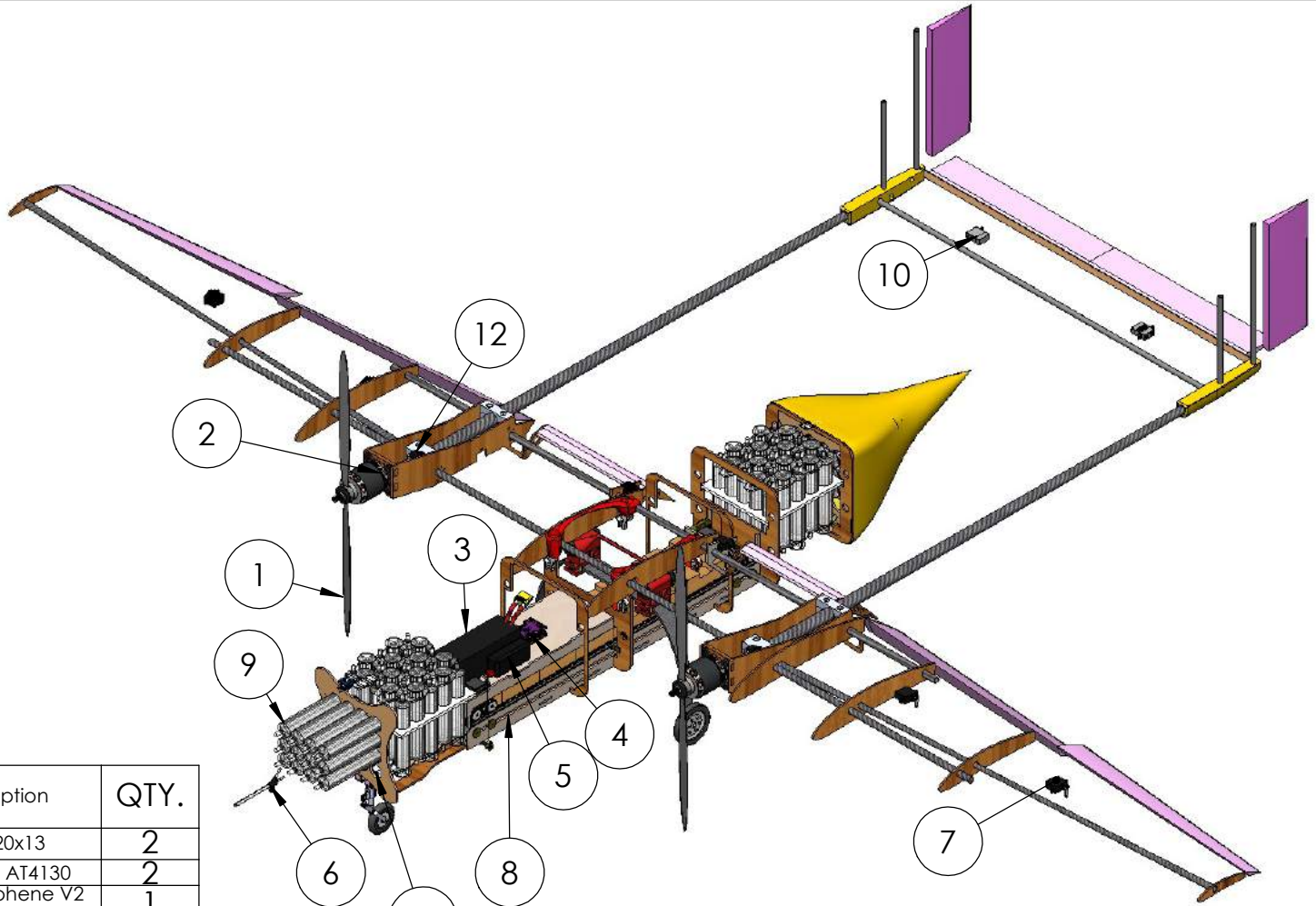
SCALE: 1:10 Drawing Package SHEET 2 OF 4

2

1

B

B



Part NO.	Name	Description	QTY.
1	Propellor	APC 20x13	2
2	Motor	TMOTOR AT4130	2
3	Propulsion Battery	SMC Graphene V2 4500mAh 6S 40C	1
4	Flight Controller	MATEKSYS H743- WING V2	1
5	Avionics Battery	Lumenier 1300mAh 3S	1
6	Pitot Tube	MATEKSYS ASPD-4525	1
7	Wing Servo	Corona DS 843 MG	6
8	Mission 3 Mechanism	2 Parallax Feedback 360 Servo	1
9	Syringe	30 ml	78 (Max)
10	Horizontal Stabilizer Servo	Corona DS 843 MG	2
11	Rudder Servo	Corona DS 843 MG	2
12	Nose Gear Servo	EMAX ES08MDII 12 g Metal Gear	1

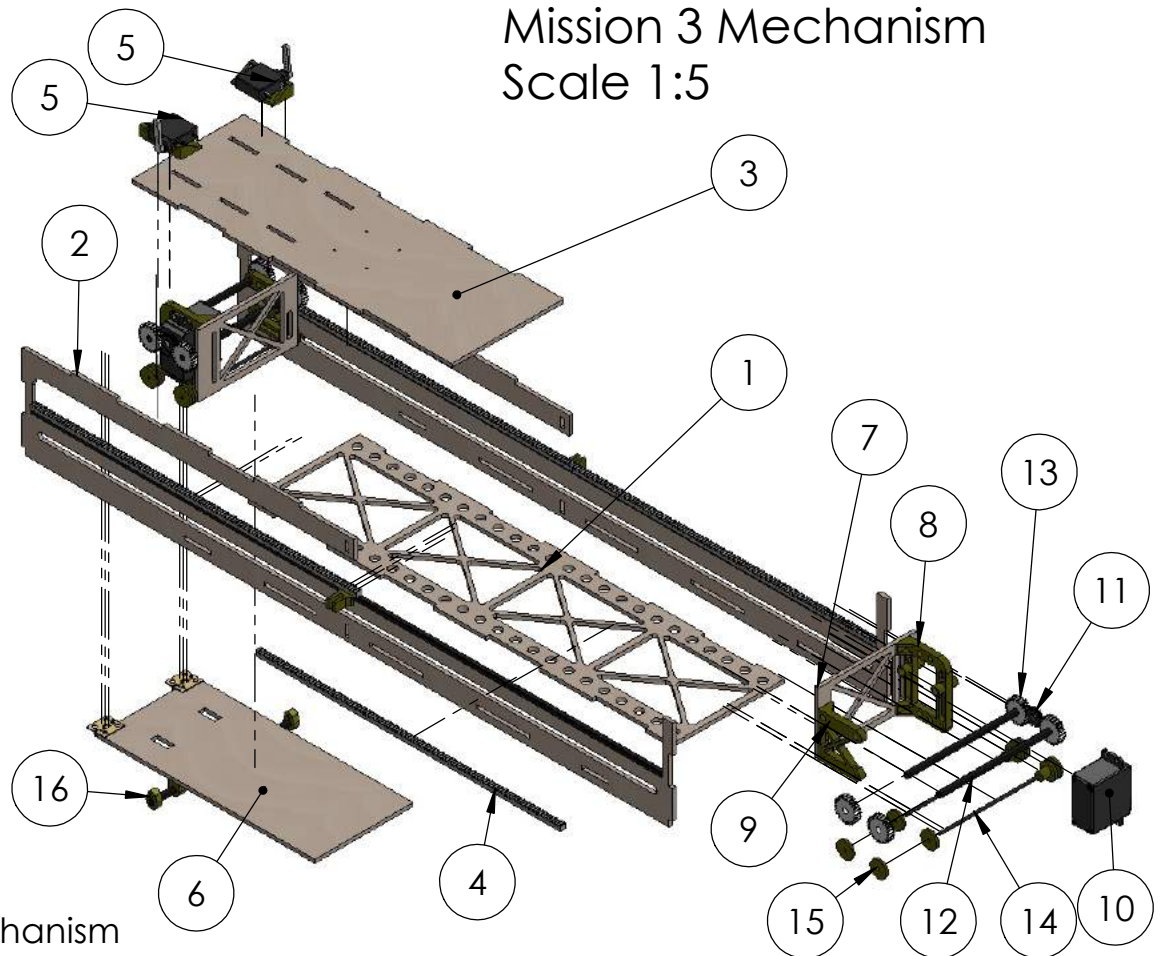
A

A

UNLESS OTHERWISE NOTED: DIMENSIONS ARE IN INCHES		HuskyWorks	
University of Washington Design/Build/Fly 2022			
TITLE: <h1>Albatross</h1>			
SIZE	DWG. NO.		
A	Systems Diagram		
SCALE: 1:10	Drawing Package	SHEET 3 OF 4	

1

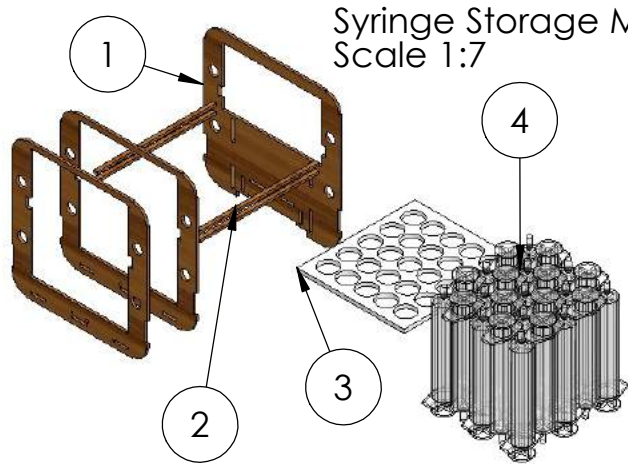
Item NO.	Name	Description	QTY.
1	Bottom Plate	Laser Cut Plywood	1
2	Side Plate	Laser Cut Plywood Strengthened with Carbon Fiber Strips	2
3	Top Plate /Battery Mount	Laser Cut Plywood	1
4	Gear Rack	Nylon	4
5	Ramp Servo	Corona 5 gram	2
6	Deployment Ramp	Laser Cut Plywood and 2 Brass Hinges	1
7	Cart Plate	Laser Cut Plywood	2
8	Shaft and Servo Mount	PLA	2
9	Shaft Mount	PLA	2
10	Cart Servo	Parallax Feedback 360	2
11	Motor Gear	Nylon	2
12	Drive Shaft	Carbon Fiber	2
13	Drive Gears	Nylon	8
14	Idler Shaft	Carbon Fiber	2
15	Idler Wheel	PLA	8
16	Ramp Control Arm	Carbon Fiber with PLA Attachments	1



Mission 3 Mechanism
Scale 1:5

B

B



Syringe Storage Mechanism
Scale 1:7

A

A

Item NO.	Part Name	Description	QTY.
1	Fuselage Ribs	Laser Cut Plywood	3
2	Tray Supports	Laser Cut Plywood	4
3	Syringe Tray	Laser Cut Foam board	1
4	Syringe	30 ml	25

UNLESS OTHERWISE NOTED: DIMENSIONS ARE IN INCHES		HuskyWorks	
University of Washington Design/Build/Fly 2022			
TITLE: Ablatross			
SIZE A	DWG. NO. Internal Mechanisms		
SCALE: 1:5	Drawing Package	SHEET 4 OF 4	

6 Manufacturing Plan

6.1 Manufacturing Processes Investigated

6.1.1 Composites

The use of composite materials such as carbon fiber has commonly been considered for design constraints in which a material with high specific strength would be optimal. While composite layups for parts such as wings and fuselage would allow for the aircraft to undergo greater load before failure, the downsides of increased time, cost, and complexity associated with a wing/fuselage make it improbable for use in some applications.

6.1.2 Laser-Cutting

Laser cutting is ideal for projects requiring quick precise 2D cuts of thin wood and foam. It is ideal for the use of structural bulkheads and ribs, as well as for hotwire cutting stencils. Laser cutting is not ideal for 3D parts with complex geometry.

6.1.3 3D-Printing

3D printing allows for the physical prototyping and manufacturing of 3D CAD models. Often used for topologically optimized parts, 3D printing allows the team to manufacture parts with complex geometry. The quality and integrity of 3D printed structures are influenced by the type of filament, the slicer settings used for the print, and the print orientation.

6.1.4 Covering Film

Covering film, combined with the use of plywood and balsa wood, can be used to make light-weight structures for both the fuselage and wings. An iron can be used to shrink and adhere the film to the wood, creating a smooth surface for aerodynamics.

6.1.5 Hotwire-Cutting

The hot wire cutter operates by sending a current through a thin strand of wire which generates heat. This is a cheap and time-efficient way to shape XPS foam and other similar materials. This year, the team explored the use of a CNC hotwire cutter, which would automate the process done previously by hand. Additionally, the minimal experience needed to operate the hotwire cutters is ideal. All of these benefits yield hotwire cutting to be one of HuskyWorks' primary manufacturing methods.

6.1.6 Machining

The use of a manual mill or lathe can be used to produce high-tolerance parts. This technique allows for processing of other high strength materials at the cost of large setup times.

6.1.7 Vacuum Forming

Vacuum Forming PET plastic was used to manufacture lightweight parts with little structural loads. The process heats up thin plastic sheets while a mold is pushed through. When the part cools down, it creates thin, somewhat flexible shells.

6.2 Manufacturing Processes Selected

Fig. 32 shows the materials used in the construction of the *Albatross*. Materials and manufacturing processes were selected based on available resources, cost, time, and complexity.



Figure 32: *Albatross* Materials Selected

6.2.1 Fuselage

The fuselage was constructed with a combination of birch plywood bulkheads, balsa wood stringers, covering film, and carbon fiber rods. Two unidirectional carbon fiber rods ran the length of the fuselage, interfacing with laser cut bulkheads placed in high stress areas. The main shape of the fuselage was formed by covering film heat-shrunk around the ribs and stringers. Ribs were laser cut from 1/8 in birch plywood, and secured into position on 1/2 in carbon fiber rods using glue. During assembly of the fuselage, the wing mounts and landing gear mounts which interface with the spars were slid into place and glued or clamped.

To support the covering film on the corners of the fuselage, stringers were made of balsa wood and layered with fiberglass to provide extra bending resistance and a surface for the film to adhere to. This prevented the covering film from curving inwards on the corners of the fuselage when shrunk, improving the aerodynamic streamline of the fuselage as a whole. Stringers were bent into a rounded shape to follow the curvature of the fuselage using a jig created with a carbon fiber rod and laser cut birch plywood rings shown in Fig. 33a. Water was applied to a 1/32 in sheet of balsa using a paper towel, and the sheet was then bent to shape around the plywood rings. The

balsa was held in the curved position using a tightened nylon string. After 2 hours of drying, the balsa was cut to shape using a knife, and 0.75 oz fiber glass was applied via a wet layup. Once the stringers were completely dry and the fiber glass had set, they were cut to size and secured to the fuselage using polyurethane glue. The next step in the process was to heat shrink the covering film around the fuselage; however, due to a need to access electronics and the deployment mechanism, this step was performed just before systems checks.

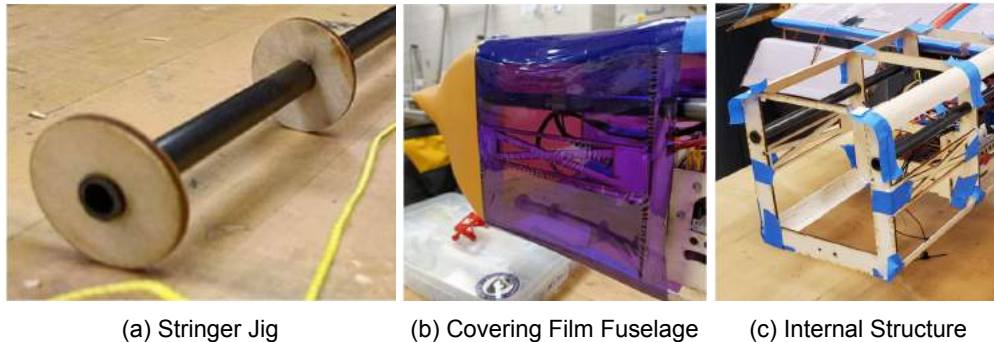


Figure 33: Fuselage Manufacturing Process Images

6.2.2 Wing and Tail

The general process for the construction of wing sections for the *Albatross* was using laser cut wooden stencils and a hotwire to cut wing sections out of XPS foam into the desired wing shape. Laser cut wooden ribs and carbon fiber spars were inserted into the foam to provide the necessary structure in the wing. Fiberglass was laid up on the wing to provide torsional rigidity.



Figure 34: Contoured Foam Wing Sections

The wing was made in three sections: left, center, and right. The center wing section was constructed in a multi-step process starting with laser cutting 2, 1/8 in birch plywood stencils to the shape of the selected airfoil and gluing the stencils to a 2 in piece of foam sized for the center section. A manual hotwire cutter was used to cut the foam to the shape of the stencils. Channels for wires were cut after the aerodynamic shape was completed.

The center section was cut into three shapes to insert the wing mount. A bandsaw-style hotwire cutter was used to cut holes for the mount. The mount was glued to a wooden rib in the foam. Fiberglass was laid up onto the surface after the mount was inserted. Fig. 35 shows the completed center section wing mount. The wing section was placed in a vacuum bag as shown in Fig. 36 to cure for two hours to obtain a smooth surface finish and remove excess resin. To complete the assembly of the center wing section, carbon fiber spars were glued into position in the ribs and wing mount, and motor mounts were glued on to the outer edges of the wing section. The left and right wing were built using the same process as the center section, with additional challenges due to the taper. When hot wire cutting these sections, two different sized stencils were used to obtain the desired taper angle. When cutting using these stencils, one side of the hotwire was moved at a different speed than the other to ensure a smooth, even cut was made. General control surfaces were made using a hotwire cut foam core layered in 1/32 in balsa wood adhered to the surface using spray adhesive. Control horns were laser cut from 1/8 in birch plywood and a slot for the horn was cut into the surface using a hand held foam cutting tool. The control horns were then glued into place using polyurethane glue. The slotted flaps were constructed using a laser cut 1/8 in birch plywood rib on either side with a foam core hotwire cut to the correct contour spanning between the ribs.

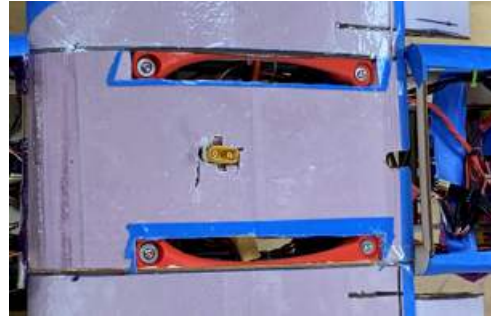


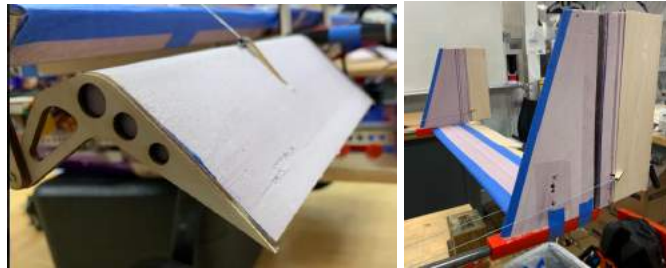
Figure 35: Center Wing Section with Mount



Figure 36: Vacuum-bagged Wing

The main shapes of the vertical and horizontal stabilizers were cut using a hotwire cutter and stencil method similar to the method used to cut wing sections. 3D printed pieces served as the joints between the foam surfaces creating the *Albatross's* U-shaped tail. Carbon fiber rods were inserted into channels cut with the hotwire to provide

structure to the foam pieces and serve as the backbone of the tail structure. The rudders on the tail were controlled using Kevlar strings connected to servos mounted on the main wing section in the motor mounts. Channels for wires and holes for servo motors were cut using a Dremel tool with a router attachment.



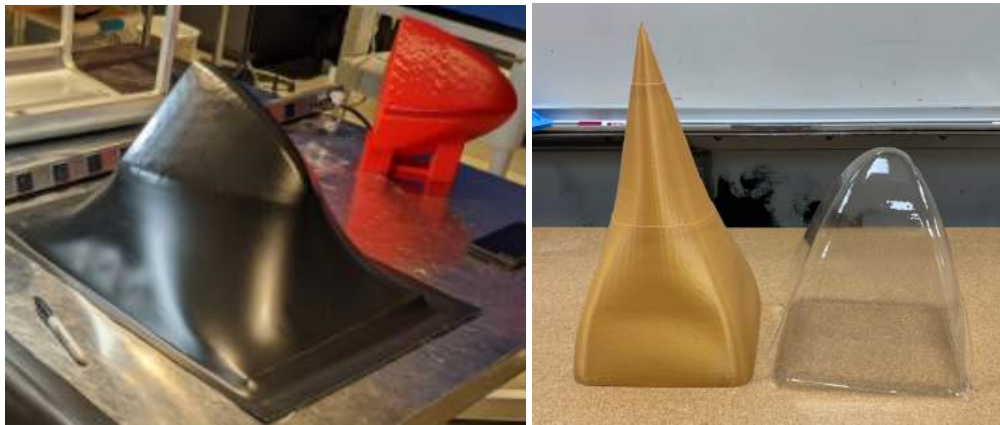
(a) Slotted Flaps

(b) Tail Assembly

Figure 37: Control Surfaces and Tail Assembly

6.2.3 Aerodynamic Cowlings

The primary aerodynamic cowlings on the Albatross were the nose and empennage. Both of these cowlings were made of with a combination of vacuum formed PET plastic and 3D printed PLA. The tip of the nose cone was made of vacuum formed plastic while the rest of the nose was made of 3D printed PLA. The empennage was entirely 3D printed. Slicer settings were changed for the nose and empennage prints to get a single layer thick print with no infill, significantly reducing the weight of the part. In both the nose and empennage, holes were drilled for screws to mount hinges connected to the fuselage. 3D printed latches were also attached using polyurethane glue to the nose and empennage to secure them to the fuselage in conjunction with the hinges.



(a) Vacuum Forming

(b) Nose and Empennage

Figure 38: Aerodynamic Cowlings

6.2.4 Mounts

The motor mounts were laser cut out of 1/8 in plywood and glued together using spars as alignment. The wing mount was made in multiple parts out of both PLA and 6061 aluminum. The mount inserted into the foam was 3D printed. The mounts secured to the fuselage longerons were fabricated using a manual mill.



(a) Machining Process

(b) Installed Aluminum Mount

Figure 39: Aluminum Wing Mount Manufacturing

6.2.5 Payload & Deployment Mechanism

The Mission 3 deployment mechanism was laser cut out of 1/8" plywood and glued together using epoxy. Unidirectional carbon strips were glued along the span in the vertical and horizontal directions to provide stiffness.

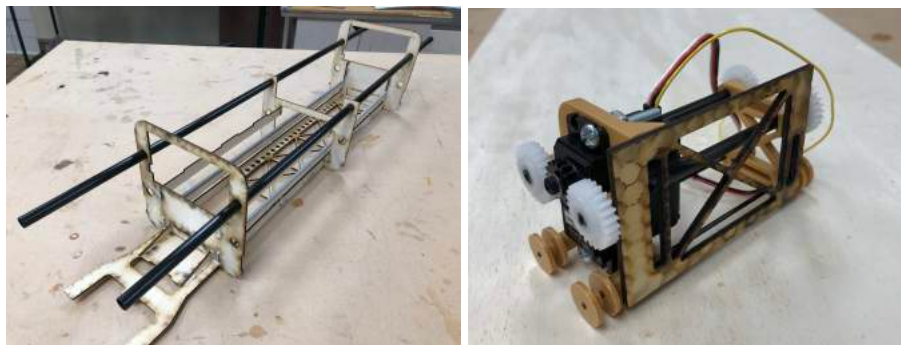


Figure 40: Payload Deployment Mechanism Frame and Package Handling Carts

6.2.6 Aircraft

Fig. 41 shows the first version of team HuskyWork's competition airframe at its first test flight.



Figure 41: Competition Aircraft Version 1

6.3 Manufacturing Schedule

Manufacturing of the *Albatross* was structured to be simple and easily repeated. With the planned construction of three aircraft: the Aerodynamic Prototype, Competition Version 1, and Competition Version 2, scheduling was mirrored from one airframe to the next. This allowed for consistent weekly schedules to keep manufacturing on time, and for processes to be streamlined and improved for each iteration of aircraft. A Gantt chart depicting the detailed manufacturing timeline is shown in Fig. 42. It should be noted that the chart includes the time taken to build the part for the first prototype, iterate and improve the design, and build it for the subsequent aircraft.

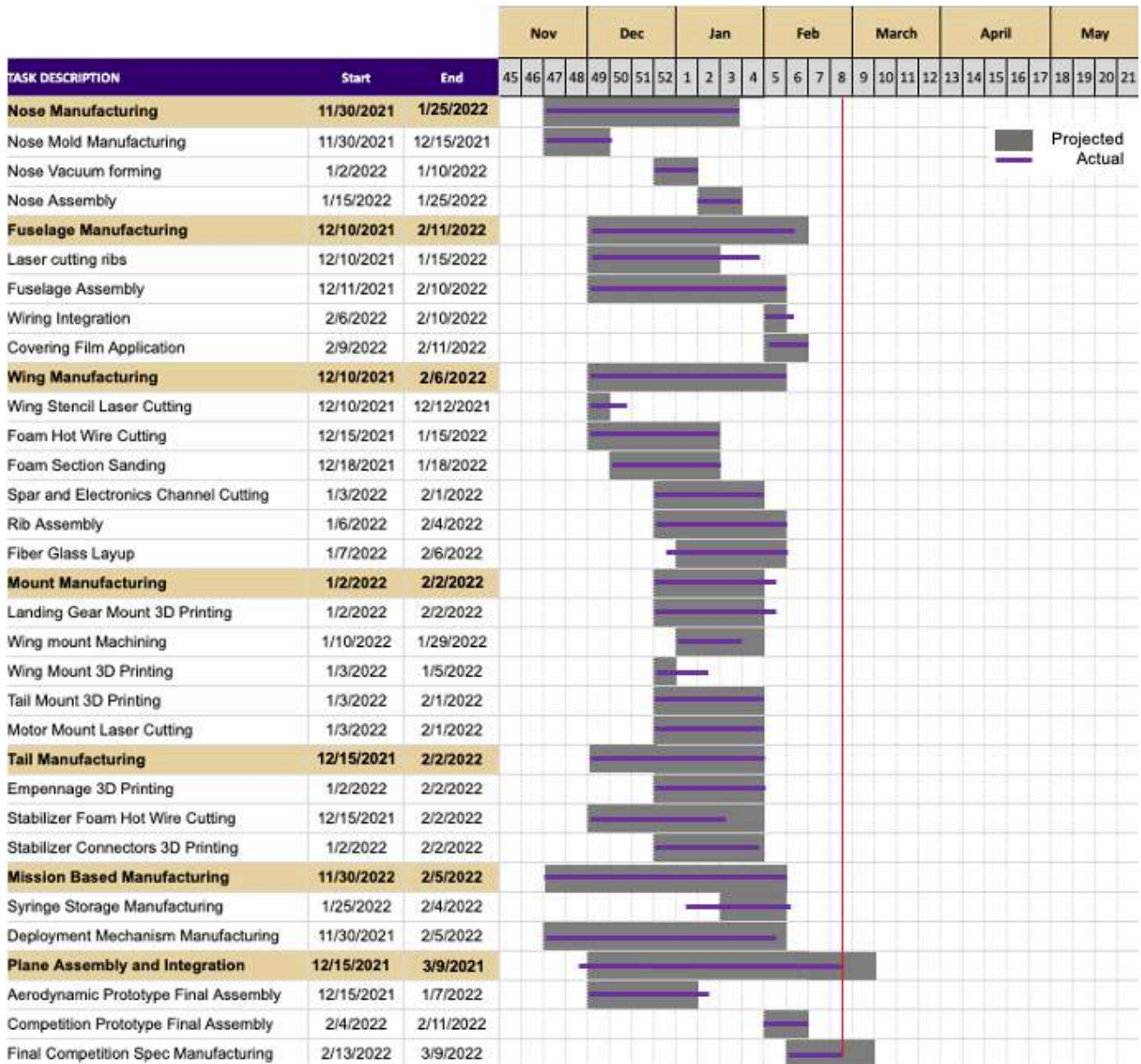


Figure 42: Manufacturing Timeline Gantt Chart

7.2.3 Propulsion

- The preliminary propulsion system was tested to demonstrate satisfactory performance during all phases of each flight mission.

7.2.4 Payload

- A fuselage drop test was performed including a vaccine package to verify that the 25G shock sensor would not trip upon an impact force, such as landing.
- Extensive mechanical testing was performed on the Mission 3 deployment mechanism to guarantee reliability of electronics and code.
- Mission 2 and 3 flight simulation test will be performed to verify aircraft performance for STOL with maximum payload and repeated takeoffs and landings.

7.3 System Testing

7.3.1 Aerodynamics Testing

Tests were performed in a 3 ft x 3 ft wind tunnel to test the aerodynamic properties of the designed body including lift, drag, and pitch moment. The test model was 3D printed with PLA, PETG, and PC, sanded and reinforced with aluminum and steel spars. In order to better simulate free-flight within the limited size of the wind tunnel, a 50% scale, half-body design was chosen. Given the scale model, the Reynold's number estimated for M3 conditions was matched. The half-body was mounted with its xz-plane (body axes) cut plane parallel to the tunnel floor, attaching to the ATI Mini 45-E balance and rotation table allowing for angle of attack variation. The tested angles of attack were between -5° and 12.5° . Yaw and roll variations were not tested.



Figure 44: (a) Airframe half-body mounted vertically in wind tunnel and (b) motor-propeller propulsion test apparatus

The C_D measured in the wind tunnel did not match results from AVL and OpenVSP, as seen in Fig. 10a. During flow-on testing, the measured axial force was lower than expected relative to the tare value and suggested

potential contact between the model-attached fairing under the splitter plate and the tunnel floor due to installed tolerances. In Fig. 10b, the lift-to-drag curve was observed to have a similar slope compared to AVL and Open-VSP. This was seen as a correct prediction, as the slope of the drag polar seen in Fig. 10a is L/D , meaning that the lower slope would translate to a lower α vs. L/D curve.

The effects of the endplates were observed to be minimal on the C_L of the plane, as seen in Fig. 11. Endplate (c) exhibited a lower slope, but it was noted in the data that the axial force tare was significantly lower than the previous cases, this difference in axial force impacting the C_L for the endplate (c) curve. Based on the error present in taking α values due to low tolerances of the force balance turning mechanism, it was deemed that there would be little benefit to choosing an endplate design based on the available data.

7.3.2 Propulsion Testing

Wind Tunnel Testing

To compare against performance predicted by eCalc, max power performance of the T-Motor AT4130 300 KV and APC 20X13E prop was measured in the wind tunnel. Thrust and torsion were measured with respect to airspeeds from 0 to 88.58 ft/s, supplying aircraft performance calculations and motor mount design with more accurate data.

In-Flight Testing

Flight tests were conducted to evaluate the overall performance of the propulsion system if calculations based on wind tunnel data suggest they were feasible. Mission simulations and various flight scenarios were conducted to obtain data from the field and from telemetry.

7.3.3 Structural Testing

A wing structure test was designed to validate the finite element analysis performed on the wing structure through testing to the max loading condition that the wing could experience (2.5G wing tip load). Due to the complexities of the tapered spars, the FEA could not generate reliable results for realistic loading cases. One outer wing section, identical to that of the competition aircraft, was constructed for this test. The outer wing was selected due to the fact that it only included one carbon fiber spar, indicating that it was the weakest part of the wing in terms of bending rigidity. Additionally, due to the taper, the wing tip is more critically loaded in shear.

The test performed was an incremental static loading test. The first objective of this test was to record the degree of deflection of the wing for multiple applied loads. The second objective of this test was to test if this wing section could withstand and recover from load equal to 2.5G at wing tip. A test stand was constructed to secure the wing section in place such that it extrudes over the edge of a table. A bucket was attached to the tip of the wing and water was poured into the bucket in 4 oz increments.

7.3.4 Package Deployment Mechanism Testing

During Mission 3, the package deployment mechanism must reliably deploy packages quickly without getting jammed. To ensure the reliability and speed of the deployment mechanism, the mechanical parts of the deployment mechanism were tested as shown in Fig. 45. The mechanical design of the package handling carts was tested using a very simple method. The package handling carts were mounted inside the frame and connected to a servo tester. A PWM control signal was manually sent to the package handling cart via the servo tester such that the carts would travel along the frame in either direction. This method of testing was used to verify proper gear meshing and smooth movement of the package handling carts. The servos were also tested for adequate performance by pushing a weight of 3 lb (six packages worth of weight) along the length of the frame. This would verify that the servo could indeed push the boxes the desired speed without stalling.



Figure 45: Mission 3 Testing: 2 Packages

7.4 Flight Tests

7.4.1 Flight Test Airframes

Three design iterations were used to evaluate the flight performance of the *Albatross*, as summarized in Tables 19 and 20. Using multiple airframes of increasing capability allowed both lessons from the test flight program and improvements in the manufacturing process to be included in the final design.

Table 19: Airframe Features

Feature	Prototype	Competition V1	Competition V2
Fuselage Skin Material	Foam Board	Covering Film	Covering Film
Horizontal Stabilizer Position	High	Low	Low
Mission 3 Hardware Installed	No	Yes	Yes
Mission 3 Mechanism Works	No	No	Yes
Syringe Mounting Hardware	No	Yes	Yes
Wheel Runway Type	Grass	Grass	Paved
Wheel Brakes	No	No	Yes



(a) Aerodynamic Prototype in Flight



(b) Competition V1 in Flight

Figure 46: Airframes in Flight

Table 20: Airframes Tested

Production Order	Airframe	Description	First Flight
1	Prototype	Designed for simplicity, the prototype flew with the same configuration and weight as the final aircraft design but with simpler and heavier construction. This design allowed the pilot to gain experience with the aircraft before subsystems were ready to be installed. Designed to operate off of a grass runway.	1/9/22
2	Comp V1	First attempt at subsystem integration, included mission 3 mechanism but mechanism was not functional due to manufacturing defects. Enabled design refinement for final competition aircraft. Designed to operate off of a grass runway.	2/13/22
3	Comp V2	The final, fully-functional competition aircraft. Designed to operate off of a paved runway.	TBD

7.4.2 Flight Test Schedule

Table 21: List of Flight Test Objectives

Flight*	Date	Airframe	Objectives	Completed
1	1/9/22	Prototype	- Trim Aircraft for comfortable cruise with flaps - Practice Approaches to predict landing behaviour - Calculate estimated flight endurance from remaining battery	Yes
2	1/9/22	Prototype	- Demonstrate predicted endurance with 20% safety margin	Yes
3	1/22/22	Prototype	- Observe full power takeoff roll (no flaps) against 25ft marker - Demonstrate takeoff flap functionality and set trim with flaps - Practice approaches with takeoff flaps - Get live telemetry to ground crew	Yes
4	1/22/22	Prototype	- Test stall characteristics with flaps up, takeoff flaps - Test high speed performance - Observe live stall, cruise, maximum, and landing speeds	Yes
5	1/22/22	Prototype	- Observe full power takeoff with takeoff flaps - Single-lap takeoff and landing circuits for landing practice	Yes
6	1/22/22	Prototype	- Backup pilot in-air training	Yes
7	1/29/22	Prototype	- Demonstrate landing flaps functionality and trim for flap setting	Yes
8	1/29/22	Prototype	- Practice landings with landing flap setting - Observe ground roll using landing flap setting	Yes
9,10	1/29/22	Prototype	- Backup pilot training for all flight phases	Yes
11	1/29/22	Prototype	- Trim aircraft at all flap settings	Yes
12	2/13/22	Comp V1	- Complete trim adjustment at all flap settings	Yes
13	2/13/22	Comp V1	- Demonstrate flight with 50% of maximum payload - Observe full power, takeoff flap ground roll against 25ft mark - Determine if lowered horizontal stabilizer improved takeoff	Yes
14, 15, 16	2/26/22	Comp V1	- Demonstrate flight at maximum takeoff weight - Observe ground roll at maximum takeoff weight - Refine trim settings for approach and landing phases - Practice landings	No
17	3/9/22	Comp V2	- Full integration ground test only - Observe effectiveness of wheel brakes on pavement - Demonstrate package deployment between taxi movements	No
18, 19, 20	3/12/22	Comp V2	- Trim new airframe at all flap settings - Takeoff and landing practice on a paved runway - Practice stopping in a target area - Full mission 2 flight simulation - Full mission 3 deployment circuits simulation	No

* A flight is defined as the use of one battery, not takeoff and landing cycles

Preflight		Before Takeoff	
ASSEMBLY		Propellers	TIGHTENED
Wings, Nose, Tail, Gear	SECURE	Propeller Area	CLEAR
Flight and Avionics Batteries	SECURE	Arming Plug	INSTALL
Center of Gravity	FRONT SPAR	Throttle Inhibit Switch	OFF
AVIONICS		Throttle	RUN UP TO 80%
Transmitter	ON	Wheel Brakes	ACTIVE
Throttle Inhibit Switch	ON	Nose Wheel Steering	ACTIVE
Arming Plug	REMOVED	Flaps	TAKEOFF
Receiver Connections	CHECKED	Elevator Throw	LOW RATES
Avionics Battery	CONNECTED	Rudder Mix	ENABLED
Flight Battery	CONNECTED	Takeoff Area	CLEAR
Access Hatch	CLOSED	Takeoff Intentions	ANNOUNCED
Avionics Power Switch	ON	After Landing	
Failsafe	CHECKED	Throttle Inhibit Switch	ON
Range	CHECKED	Arming Plug	REMOVE
AIRFRAME		Avionics Switch	OFF
Payload	SECURE	Flight Battery	DISCONNECT
Ramp	CLOSED	Avionics Battery	DISCONNECT
Center of Gravity	FIRST SPAR	Radio Power	OFF
Landing Gear Roll	SMOOTH	Aircraft Structure	INSPECT
Control Surfaces	SECURE		
Control Inputs	CORRECT		
Trims	CHECK		

8 Performance Results

8.1 Demonstrated System Performance

8.1.1 Propulsion Testing Results

The graph shown in Fig. 47 was produced from the results of the wind tunnel thrust test.

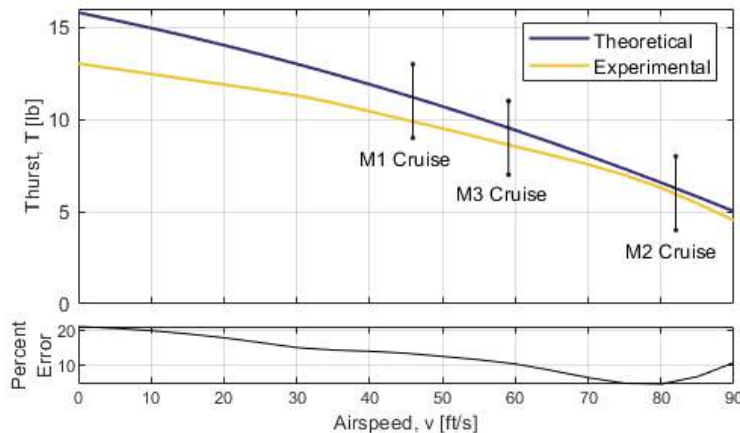


Figure 47: T-Motor AT4130 300 KV + APC 20X13E Dynamic Thrust Performance at 3000 Watts

While the M2 thrust performance is satisfactory, according to Fig. 47, an 18% average thrust deficit to eCalc predictions was measured during the takeoff regime from 0 to 40 ft/s. Since the AT4130 was the most powerful of its class, it was deduced that other motors may suffer the same deficit. With larger motors requiring significant structural changes, the AT4130 was elected to continue flight test to progress other testing programs, while a backup solution was investigated in case more thrust was needed.

General flight performance and M3 performance were both evaluated directly by conducting flight tests. The pilot was instructed to fly under 900 Watts of power after takeoff, with average airspeed, and flight time (excluding landing sequence) recorded. 3 flights were conducted in this manner, with an average airspeed of 42 ft/s and an average flight time of 6 minutes 48 seconds. Distance equivalent to 8 competition laps was obtained through conservative calculations. Since all flights landed with at least 15% propulsion energy remaining, enough to account for energy consumption of 6 takeoffs, M3 propulsion performance was considered satisfactory. Pilot feedback was positive on the responsiveness and acceleration provided by propulsion, and zero failures were suffered by the APD ESCs after more than 30 takeoffs and landings. Lastly, during flight test of Competition V1, takeoff within 25 ft was achieved using the AT4130 motor at half payload with more than 3 ft to spare. Since takeoff performance is expected to improve on Competition V2 with better landing gear placement, combined with calculations, takeoff performance from the AT4130 was considered sufficient. Therefore, due to their satisfactory performance, all components from preliminary propulsion design were finalized.

8.1.2 Structural Testing

Given an applied load of 13.1 lb added incrementally, the wing deflected 15° without any visible structural damage. This test simulated the bending moment at the inboard side of the wing, validating the structure's ability to withstand this load. After this was validated, the wing was loaded up to 18.75 lb to simulate a 2.5G wing tip load. The wing was observed to deflect 20° with a tip displacement of -10 in, as shown in Fig. 48. Upon inspection of the wing, minimal damage was observed.



Figure 48: Max Wing Deflection (20°)

8.1.3 Payload Deployment Mechanism Design

The initial test of the package handling carts did not successfully demonstrate proper gear meshing or smooth movement of the carts. It was determined that larger gear teeth would be necessary to ensure proper gear meshing. The gear pitch size was changed from 48 to 32 for all subsequent designs and tests. In subsequent tests, it was found that two gears running along the gear racks were needed to mitigate the twisting motion caused by the servo torque. After several iterations, the final package handling cart design could reliably move

the full length of the deployment mechanism. It was also verified that the carts could move at approximately one box length per second as desired. With the final iteration of the package handling carts, the deployment mechanism could reliably push 3 lb of payload at the desired speed, verifying the mechanical design of the package handling carts. One drop was measured to take 18 seconds.

8.2 Flight Performance

8.2.1 Flight Test Outcomes

Table 23 details the events that took place during each field test. Table 24 compares values measured in flight to their predicted analytical counterparts. Airspeed was read in real time using a pitot tube, which was downlinked via telemetry to a headset worn by a Ground Crew Member. Load factor was downlinked live from an onboard Inertial Measurement Unit (IMU), and time was recorded with a phone stopwatch. Fig. 49 shows the view of the Ground Crew Member during flight. Red boxes indicate the relevant data collected by the team: airspeed, location, and G-loading. This allowed the team to collect the data shown in Table 24.



Figure 49: Live Telemetry On-board Competition V1 Aircraft

Table 23: Flight Test Results

Flight	Duration	Outcome	Data and Application
1	4:23	Normal takeoff* and successful landing, aircraft trimmed for comfortable cruise	- Battery after landing remained at 70-80% capacity, allowing for a conservative target flight duration of 8 minutes and reserves for further flights - Aircraft cruised comfortably at a power setting just above 50%, which is desired
2	8:15	Normal takeoff, nose wheel broke on hard landing. Endurance flight. Continued refinement of trim.	- Battery after landing remained at 20-30% of useful capacity, indicating more endurance was possible - Wing tip test qualitatively revealed the need to stiffen wings prior to high-speed flight due to the danger of flutter
3	~8m	Performance takeoff,** observed to be longer than 25ft. Takeoff flaps tested in flight and trim was set with flaps. Tip stalled on landing resulting in broken nose gear. Telemetry data demonstrated.	- Long takeoff roll was expected and can be reduced with flaps and other design changes as needed.
4	~6.5m	Stall, high-speed, and landing data successfully collected by visually observing pitot tube readout on heads-up display (See section 8, Performance Results). Performed successful stalls and high-speed passes.	- Airspeed numerical data allowed the aerodynamics team to assess the aircraft's similarity to predicted design models - Qualitative stall characteristics helped pilot understand the aircraft's approach to stall and proper recovery procedure
5,6	~6m ~8m	Backup pilot obtained cruise flight experience with the aircraft. Primary pilot practiced landing circuits. Takeoff flaps were observed to still not meet takeoff distance requirements. Repeated takeoffs and landings were practiced in each flight.	- Flight experience helped backup pilot prepare for first takeoff attempt - Landing practice reduced chances of damage to the aircraft on landing - Long takeoff roll with flaps required further evaluation with the landing flap setting
7	~4.5m	Landing flaps successfully deployed and trimmed. Aircraft lost propulsion power due to loading of a drained flight battery and landed in tall grass, breaking the nose gear.	- The additional 4:30 flight time of the drained battery from a previous flight gave an indication of reserve time available over the 8:00 target flight time
8	~5m	Performance takeoff executed with landing flaps. Aircraft was observed to lift vertically off the ground rather than rotate during takeoff, resulting in longer ground roll. Successful landing practice with full flaps.	- Vertical lift-off behavior indicated a lack of pitch authority to pitch the nose up quickly for takeoff. This was addressed by lowering the horizontal stabilizer into the prop wash in the next version of the aircraft.
9,10	~4m ~5m	Backup pilot flew two complete, successful flights	None
11	~2m	Normal takeoff with flaps up, aircraft trimmed for cruise. Radio signal was temporarily lost, resulting in loss of propulsion, which continued after control was regained. The resulting hard landing with no power broke the nose landing gear.	- The loss of signal required a repositioning of antennae on the aircraft, and the throttle cut behavior necessitated a complete replacement of the flight controller.
12	~6m	Trim at flap settings was successfully completed. Landed with takeoff flaps.	None
13	~6m	Performance takeoff with 50% payload weight resulted in a takeoff roll under 25ft. The aircraft rotated as intended on takeoff. Tip stall on landing broke nose gear.	- Frequent damage to the nose gear inspired the repositioning of the main landing gear closer to the center of gravity to reduce nose gear loads.

* A normal takeoff means power is eased up to near 80% with no attempt to minimize ground roll

** A performance takeoff means full power is applied immediately and ground roll is minimized

Table 24: Demonstrated Flight Performance

Parameter	Flight Test	Analytical Prediction
Empty Weight (lbs)	12.52	9.28
Stall Speed (ft/s)	32.8	37.59
Max Demonstrated Speed (ft/s)	78.38	78.72
Cruise Speed (ft/s)	42.65	59.06
Approach Speed (ft/s)	36.45	-
Touchdown Speed (ft/s)	27.34	-
Maximum Observed Load Factor	2.5	-
Flight Endurance (min)	9:54*	10:00
Takeoff Goal Met?	No	Yes

* Flight endurance extrapolated from 20% remaining after 8:15 flight.

8.2.2 Design Modifications Due to Flight Testing

Takeoff performance and weight drove the largest performance-based changes to the design. As shown in Table 24, empty weight came in significantly higher than the objective due to extra weight from modifications during manufacturing and the addition of monitoring equipment. The ground roll with the original design was observed to be too long, and the aircraft was not able to rotate early for takeoff due to insufficient elevator authority. To address this observation, the following changes were made:

- The fuselage was redesigned from the Prototype to Competition V1 using plastic covering film, which offers a slight weight advantage over foam board.
- The horizontal stabilizer was lowered from a high tail down into the propeller wash to increase airflow over the elevator at takeoff power and allow the nose to be raised earlier.
- The main landing gear was moved closer to the center of gravity to reduce the moment arm between the gear and the center of gravity to enable the elevator to raise the nose earlier with less force.

Fig. 50 shows the Competition V1 aircraft proof of takeoff within 25 ft the modified tail. The orange cone in the image represents the 25 ft mark. Fig. 51 shows the Competition V1 aircraft in turning flight.



Figure 50: Proof of Takeoff within 25 ft



Figure 51: Competition V1 Aircraft in Flight

References

- [1] Raymer, D., *Aircraft Design: A Conceptual Approach*, American Institute of Aeronautics and Astronautics, Inc., 6th ed., 2018.
- [2] Mueller, M., "PROPCALC," Feb 2022.
- [3] *Airfoil Tools*, 2020.
- [4] Nicolai, L. and Carichner, G., *Fundamentals of Aircraft and Airship Design*, Vol. 1, American Institute of Aeronautics and Astronautics, Inc., 2010.
- [5] ramcdona, *Parasite Drag Tool*, OpenVSP, May 2020.
- [6] Anderson, J., *Introduction to Flight*, McGraw-Hill Education, New York, NY, 8th ed., 2016.
- [7] Aug, MIL-F-8785C.
- [8] MCSGuy, "Lipo Battery Testing Comparisons as of Oct. 2021," *RC Groups RSS*, May 2021.
- [9] *AT3530 Long Shaft*, T-Motor, 2020.